

AWARD NUMBER: W81XWH-14-1-0068

TITLE: Defining Translational Reprogramming in Tuberous Sclerosis Complex

PRINCIPAL INVESTIGATOR: Shu-Bing Qian

CONTRACTING ORGANIZATION: Cornell University
Ithaca, NY 14850

REPORT DATE: July 2016

TYPE OF REPORT: Annual Report

PREPARED FOR: U.S. Army Medical Research and Materiel Command
Fort Detrick, Maryland 21702-5012

DISTRIBUTION STATEMENT: Approved for Public Release;
Distribution Unlimited

The views, opinions and/or findings contained in this report are those of the author(s) and should not be construed as an official Department of the Army position, policy or decision unless so designated by other documentation.

REPORT DOCUMENTATION PAGE				Form Approved OMB No. 0704-0188	
Public reporting burden for this collection of information is estimated to average 1 hour per response, including the time for reviewing instructions, searching existing data sources, gathering and maintaining the data needed, and completing and reviewing this collection of information. Send comments regarding this burden estimate or any other aspect of this collection of information, including suggestions for reducing this burden to Department of Defense, Washington Headquarters Services, Directorate for Information Operations and Reports (0704-0188), 1215 Jefferson Davis Highway, Suite 1204, Arlington, VA 22202-4302. Respondents should be aware that notwithstanding any other provision of law, no person shall be subject to any penalty for failing to comply with a collection of information if it does not display a currently valid OMB control number. PLEASE DO NOT RETURN YOUR FORM TO THE ABOVE ADDRESS.					
1. REPORT DATE July 2016		2. REPORT TYPE Annual Report		3. DATES COVERED 1 Jul 2015 - 30 Jun 2016	
4. TITLE AND SUBTITLE Defining Translational Reprogramming in Tuberous Sclerosis Complex				5a. CONTRACT NUMBER	
				5b. GRANT NUMBER W81XWH-14-1-0068	
				5c. PROGRAM ELEMENT NUMBER	
6. AUTHOR(S) Shu-Bing Qian E-Mail: sq38@cornell.edu				5d. PROJECT NUMBER	
				5e. TASK NUMBER	
				5f. WORK UNIT NUMBER	
7. PERFORMING ORGANIZATION NAME(S) AND ADDRESS(ES) Cornell University 373 Pine Tree Road Ithaca, NY 14850				8. PERFORMING ORGANIZATION REPORT NUMBER	
9. SPONSORING / MONITORING AGENCY NAME(S) AND ADDRESS(ES) U.S. Army Medical Research and Materiel Command Fort Detrick, Maryland 21702-5012				10. SPONSOR/MONITOR'S ACRONYM(S)	
				11. SPONSOR/MONITOR'S REPORT NUMBER(S)	
12. DISTRIBUTION / AVAILABILITY STATEMENT Approved for Public Release; Distribution Unlimited					
13. SUPPLEMENTARY NOTES					
14. ABSTRACT Inactivating mutations in the TSC1 and TSC2 tumor suppressor genes lead to the disease tuberous sclerosis complex (TSC). The TSC1/TSC2 complex integrates multiple cues to regulate protein translation and cell growth via mammalian target of rapamycin complex 1 (mTORC1). Loss of TSC functions leads to constitutive activation of mTORC1 and uncontrolled mRNA translation. In recently published data, we discovered that TSC2-deficient cells have increased protein synthesis but with reduced protein quality, leading us to hypothesize that disrupted protein homeostasis contributes to TSC pathophysiology. Consistent with this hypothesis, in unpublished data, we have found prevailing alternative translation that re-shapes proteome landscape. Our results suggest that translational re-programming can be targeted for therapeutic strategies					
15. SUBJECT TERMS Tuberous sclerosis complex; mTORC1; rapamycin; mRNA; translation; ribosome; quality control; alternative translation					
16. SECURITY CLASSIFICATION OF:			17. LIMITATION OF ABSTRACT	18. NUMBER OF PAGES	19a. NAME OF RESPONSIBLE PERSON
a. REPORT	b. ABSTRACT	c. THIS PAGE			USAMRMC
Unclassified	Unclassified	Unclassified	Unclassified	30	19b. TELEPHONE NUMBER (include area code)

Table of Contents

	<u>Page</u>
1. Introduction.....	1
2. Keywords.....	2
3. Accomplishments.....	3
4. Impact.....	6
5. Changes/Problems.....	7
6. Products.....	8
7. Participants & Other Collaborating Organizations.....	9
8. Special Reporting Requirements.....	10
9. Appendices.....	11

1. INTRODUCTION

Tuberous sclerosis complex (TSC) is an autosomal dominant disease characterized by benign tumors in various tissues. The genes mutated in this disease, TSC1 and TSC2, encode tumor suppressors that are associated in a complex. The TSC1/2 complex, through its Rheb-GAP activity, is a critical negative regulator of mTORC1 under physiological conditions. Activation of mTORC1 positively stimulates cap-dependent mRNA translation via its downstream substrates S6K and 4E-BP. In our previous study, we demonstrated that TSC-mTORC1 signaling regulates the balance between cap-dependent and cap-independent translation. In this project, we aim to (1) Dissect the molecular linkage between mTORC1 and protein homeostasis; (2) Define the role of mTORC1 in ribosome dynamics and translational re-programming.

2. KEYWORDS

Tuberous sclerosis complex; mTORC1; rapamycin; mRNA; translation; ribosome; quality control; alternative translation

3. ACCOMPLISHMENTS

- **What were the major goals of the project?**

Task 1. Dissect the Molecular Linkage between mTORC1 and Protein Homeostasis

Task 2. Define the Role of mTORC1 in Ribosome Dynamics and Translational Re-programming

- **What was accomplished under these goals?**

1. Dynamic m⁶A mRNA methylation directs translational control of heat shock response.

The most abundant mRNA post-transcriptional modification is N⁶-methyladenosine (m⁶A) that has broad roles in RNA biology. In mammalian cells, the asymmetric distribution of m⁶A along mRNAs leaves relatively less methylation in the 5' untranslated region (5'UTR) compared to other regions. However, whether and how 5'UTR methylation is regulated is poorly understood. Despite the crucial role of the 5'UTR in translation initiation, very little is known whether m⁶A modification influences mRNA translation. Here we show that in response to heat shock stress, m⁶A is preferentially deposited to the 5'UTR of newly transcribed mRNAs. We found that the dynamic 5'UTR methylation is a result of stress-induced nuclear localization of YTHDF2, a well characterized m⁶A “reader”. Upon heat shock stress, the nuclear YTHDF2 preserves 5'UTR methylation of stress-induced transcripts by limiting the m⁶A “eraser” FTO from demethylation. Remarkably, the increased 5'UTR methylation in the form of m⁶A promotes cap-independent translation initiation, providing a mechanism for selective mRNA translation under heat shock stress. Using Hsp70 mRNA as an example, we demonstrate that a single site m⁶A modification in the 5'UTR enables translation initiation independent of the 5' end m⁷G cap (**Fig. 1**). The elucidation of the dynamic feature of 5'UTR methylation and its critical role in cap-independent translation not only expands the breadth of physiological roles of m⁶A, but also uncovers a previously unappreciated translational control mechanism in heat shock response.

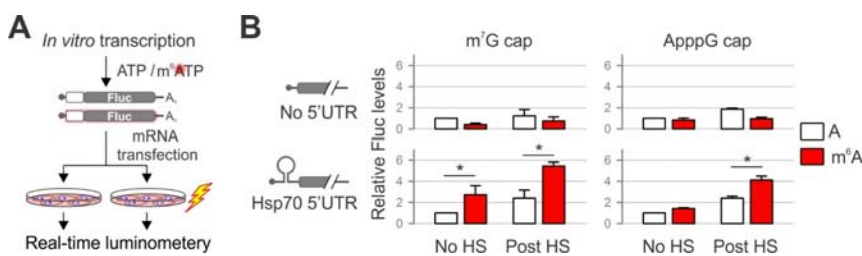


Fig 1. (A) Schematic of Fluc reporter construction and transfection. **(B)** Constructs expressing Fluc reporter with no 5'UTR or Hsp70 5'UTR are depicted on the left. Fluc activities in transfected MEF cells were quantified and normalized to the control lacking m⁶A.

2. N⁶-methyladenosine guides alternative mRNA translation in the integrated stress response.

The integrated stress response (ISR) facilitates cellular adaptation to a variety of stress conditions via phosphorylation of the common target eIF2 α . While global protein synthesis is suppressed, the translation of certain stress-related mRNAs is upregulated. The “privileged” translation often relies on alternative mechanisms, such as leaky scanning or reinitiation. However, mechanistic details of ISR-induced alternative translation remain incompletely understood. Here we report that, in response to amino acid starvation, the reinitiation of ATF4 is not only governed by eIF2 α -controlled ternary complex availability, but is also subjected to

regulation by mRNA methylation in the form of N⁶-methyladenosine (m⁶A) (**Fig. 2**). We demonstrate that m⁶A modification in the 5' untranslated region (5'UTR) controls ribosome scanning and facilitates selection of non-optimal start codons. Global profiling of initiating ribosomes reveals widespread alternative translation events influenced by mRNA methylation. By modulating the stringency of alternative initiation sites, dynamic 5'UTR methylation contributes broadly to translational regulation during ISR.

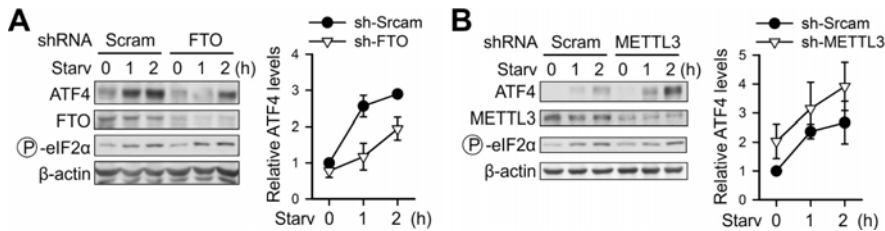


Fig 2. MEF cells with or without FTO knockdown (**A**) or METTL3 knockdown (**B**) were subject to amino acid starvation followed by immunoblotting. The right panel shows the relative ATF4 levels quantified by densitometry and normalized to β-actin.

3. Robust m⁶A-mediated cap-independent translation requires ABCF1

In eukaryotic cells, protein synthesis is typically initiated by the binding of eIF4F to the 7-methylguanylate (m⁷G) cap found on the 5' end of the majority of mRNAs. Surprisingly, overall translational output remains robust under eIF4F inhibition. The sustained protein synthesis has been attributed to cap-independent translation mediated by internal ribosome entry sites (IRESs). However, the IRES-driven translation is incompatible with the nature of eIF4F-resistant translomes. Here, we report that N⁶-methyladenosine (m⁶A)-mediated translation prevails on capped mRNAs and is resistant to eIF4F inactivation. Ribosome profiling reveals that m⁶A-facilitated translation co-exists with cap-dependent translation for a large proportion of mRNAs with a wide range of translation efficiencies. Depletion of the methyltransferase METTL3 selectively inhibits translation of mRNAs bearing 5'UTR methylation, but not mRNAs with 5' terminal oligopyrimidine (TOP) elements.

Additionally, we identify ABCF1 as a critical mediator of m⁶A-promoted cap-independent translation under both stress and physiological conditions (**Fig. 3**). Supporting the role of ABCF1 in m⁶A-mediated cap-independent translation, ABCF1-sensitive transcripts largely overlap with METTL3-responsive mRNA targets. By illustrating the scope and the mechanism of translation initiation that is neither cap- nor IRES-dependent, these findings reshape our current perceptions of cellular translational pathways. We suggest that different translation modes are coordinated to produce adaptive translomes in response to environmental and physiological stimuli.

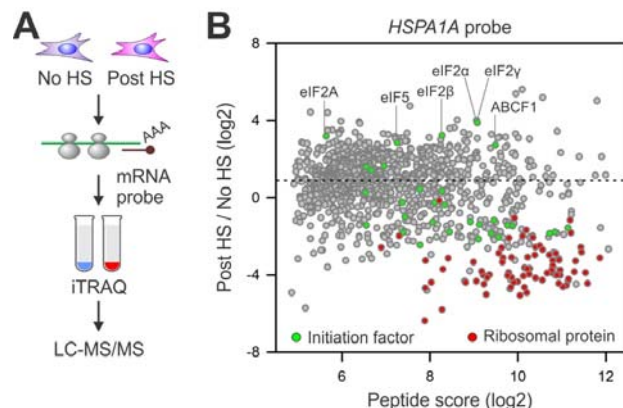


Fig 3. (**A**) Schematic of quantitative mass spectrometry. (**B**) iTRAQ results of *HSPA1A*-associated proteins in HeLa cells with or without heat shock stress. Both the peptide score (log₂) and stress-induced fold changes (log₂) are shown in the plot.

- What opportunities for training and professional development has the project provided?

Nothing to report

- **How were the results disseminated to communities of interest?**

Nothing to report

- **What do you plan to do during the next reporting period to accomplish the goals?**

1. O-GlcNAc Signaling in Translational Control of Stress Response

Translational control plays a critical role in maintaining protein homeostasis under stress conditions as it allows immediate and selective changes in protein levels. A long-standing question in the field of translational control is the mechanism through which cellular mRNAs are able to undergo cap-independent translation. How cells orchestrate differential modes of mRNA translation upon stress remains poorly understood. The goal of this project is to investigate dynamic O-GlcNAcylation in response to stress and understand its role in cap-independent mRNA translation. O-GlcNAc has been proposed to regulate diverse cellular processes, including transcription and cell signaling pathways. Our preliminary results have indicated that O-GlcNAcylation switches the function of eIF4G1 from cap-dependent to cap-independent initiation. We further uncovered a mechanistic linkage between O-GlcNAcylation, ABCF1, and mRNA methylation in cap-independent mRNA translation. These findings led to the central hypothesis that stress-induced O-GlcNAc modification of eIF4G1 licenses cap-independent mRNA translation by remodeling pre-initiation complex formation, recognizing methylated mRNA, and facilitating cap-independent translation. To test this hypothesis, the following Aims are proposed: 1) Characterize the functional switch of eIF4G1 upon O-GlcNAcylation; 2) Define the role of ABCF1 in O-GlcNAc signaling; 3) Dissect the network between mRNA methylation and O-GlcNAc signaling. These Aims are independent of one another but unified in their central focus on O-GlcNAc signaling in translational control of stress response. By integrating innovative approaches into fundamental studies of translational regulation, the proposed studies will open up new avenues of research in the field of mRNA translation. The mechanistic insights we gain from this study will provide paradigms for better understanding of translational control in cellular homeostasis and stress adaptation.

2. Linking mitochondrial tRNA modification and the proteome landscape

Mitochondrion represents an elegant example of a self-sustained system. Bearing its own genome and the translation machinery, mitochondria produces proteins necessary for ATP production. Approximately 200 pathogenic mutations have been mapped to mitochondrial tRNA (mt tRNA) genes. Chemical modifications are a characteristic structural feature of mt tRNAs which contain 16 species of modified nucleosides including three that are mitochondria-specific. Loss of modifications found at the wobble positions of mt tRNAs have been implicated in disrupted tRNA structures that may affect their translation capability. However it is still not completely understood how mt tRNA modification contributes to the regulation of the mitochondrial proteome. In particular, there is little mechanistic knowledge about the nature of crosstalk between mitochondrial activity and cellular stress signals.

To address this complex biological problem in a systematic manner, we developed innovative approaches by coupling high-resolution ribosome profiling with quantitative mapping of tRNA modification. Mridu Saikia, the new postdoc in my laboratory, hypothesized that mt tRNA modification acts as a sentinel for cellular stress signals and the altered proteome triggers mitonuclear protein imbalance and contributes to disease development. We will determine how cellular stress affects mitochondrial metabolism, map mt tRNA modification in response to stress, and define the role of mt tRNA modification in translation.

4. IMPACT

- **What was the impact on the development of the principal discipline(s) of the project?**

For years, researchers have been fixated on the idea that eukaryotic mRNA translation relies on two mutually exclusive mechanisms: cap-dependent ribosome scanning and cap-independent internal ribosome entry. Despite the predominant belief that eIF4F-mediated cap-dependent translation contributes to the majority of protein synthesis in eukaryotic cells, it is puzzling that inhibiting cap recognition by chemical inhibitors or genetic ablation only has modest effect on protein synthesis. The simplest interpretation of this conundrum is that cells rely on cap-independent initiation mechanism for substantial amount of mRNA translation. The IRES-driven translation has become essentially synonymous with 5' cap-independent mRNA translation. However, many cellular mRNAs that have been considered to contain IRESs failed to pass through stringent test for internal initiation. Additional concepts are needed to explain how cells maintain robust translation intensity during episodes of eIF4F inhibition. Here we report that m⁶A-mediated translation initiation follows a cap- and IRES-independent mechanism. Unlike IRES elements that often confer transcript specificity, the m⁶A-promoted cap-independent translation co-exists with eIF4F-mediated cap-dependent translation initiation for a great deal of transcripts. By illustrating the scope and the mechanism of translation initiation that is neither cap- nor IRES-dependent, these findings reshape our current perceptions of cellular translational pathways. We suggest that different translation modes are coordinated to produce adaptive translatoemes in response to environmental and physiological stimuli.

- **What was the impact on other disciplines?**

Nothing to report

- **What was the impact on technology transfer?**

Nothing to report

- **What was the impact on society beyond science and technology?**

Nothing to report

5. CHANGES / PROBLEMS

Nothing to report

6. PRODUCTS

- **Publications, conference papers, and presentations**

Journal publications (* Corresponding author)

1. Liu B and Qian SB*. Characterizing inactive ribosomes in translational profiling. **Translation** 2016; 4(1):e1138018. doi: 10.1080/21690731.2015.1138018.
2. Qian SB*. Step back for seminal translation. **Nat Struct Mol Biol** 2016; 23(5):362-3
3. Zhou J, Rode KA and Qian SB*. m6A: a novel hallmark of translation. **Cell Cycle** 2016; 15(3):309-10
4. Zhou J, Wan J, Gao, X, Zhang X, Jaffrey SR and Qian SB*. Dynamic m6A mRNA methylation directs translational regulation of heat shock response. **Nature** 2015; 526(7574):591-4
5. Meyer KD, Patil DP, Zhou J, Zinoviev A, Skabkin MA, Elemento O, Pestova TV, Qian SB and Jaffrey SR. 5' UTR m6A promotes cap-independent translation. **Cell** 2015; 163(4):999-1010
6. Gao X, Wan J, and Qian SB. Genome-wide profiling of alternative translation initiation sites. **Methods Mol Biol** 2016; 1358:303-16

Acknowledgement of federal support: Yes.

- **Other products**

Nothing to report

7. PARTICIPANTS & OTHER COLLABORATING ORGANIZATIONS

- **What individuals have worked on the project?**

Name: Shu-Bing Qian, PhD
Project Role: PI
Nearest person month worked: 1
Contribution to Project: Dr. Qian is responsible for the overall administration and direction of the project, including designing experimental protocols, interpreting results, writing manuscripts and supervising research assistants.

Name: Jun Zhou, PhD
Project Role: Postdoc
Nearest person month worked: 12
Contribution to Project: Dr. Zhou will be responsible for ribosome profiling experiments (Aim 1, Aim 2).

- **Has there been a change in the active other support of the PD/PI(s) or senior/key personnel since the last reporting period?**

Nothing to report

- **What other organizations were involved as partners?**

Nothing to report

8. SPECIAL REPORTING REQUIREMENTS

N/A

9. APPENDICES

Copies of journal articles

PERSPECTIVE

Characterizing inactive ribosomes in translational profiling

Botao Liu^{a,b,#} and Shu-Bing Qian^{a,b}

^aDivision of Nutritional Sciences, Cornell University, Ithaca, NY, USA; ^bGraduate Field of Genetics, Genomics, and Development, Cornell University, Ithaca, NY, USA

ABSTRACT

The broad impact of translational regulation has emerged explosively in the last few years in part due to the technological advance in genome-wide interrogation of gene expression. During mRNA translation, the majority of actively translating ribosomes exist as polysomes in cells with multiple ribosomes loaded on a single transcript. The importance of the monosome, however, has been less appreciated in translational profiling analysis. Here we report that the monosome fraction isolated by sucrose sedimentation contains a large quantity of inactive ribosomes that do not engage on mRNAs to direct translation. We found that the elongation factor eEF2, but not eEF1A, stably resides in these non-translating ribosomes. This unique feature permits direct evaluation of ribosome status under various stress conditions and in the presence of translation inhibitors. Ribosome profiling reveals that the monosome has a similar but not identical pattern of ribosome footprints compared to the polysome. We show that the association of free ribosomal subunits minimally contributes to ribosome occupancy outside of the coding region. Our results not only offer a quantitative method to monitor ribosome availability, but also uncover additional layers of ribosome status needed to be considered in translational profiling analysis.

ARTICLE HISTORY

Received 28 October 2015
Revised 20 December 2015
Accepted 28 December 2015

KEYWORDS



elongation factors; profiling;
ribosome; translation

Introduction


Translation can be divided mechanistically into 4 phases: initiation, elongation, termination and ribosome recycling.^{1,2} Eukaryotic initiation begins with the recruitment of the small ribosomal subunit (40S) to the mRNA mainly via the recognition of 5' cap structure. Following a scanning process, the selection of a start codon is accompanied with joining of the large ribosomal subunit 60S.^{3,4} The formation of 80S ribosome at the start codon is followed by repetitive elongation steps mediated by elongation factors eEF1A and eEF2. eEF1A delivers aminoacylated tRNA to the ribosomal A site, whereas eEF2 catalyzes ribosomal translocation after formation of the peptide bond.⁵ Once the 80S ribosome encounters a stop codon, termination occurs by the concerted action of release factors eRF1 and eRF3. Together with the ATP-binding cassette protein ABCE1, the terminating ribosome splits into free 60S and 40S subunits.⁶ During ribosome recycling, a new round of translation is initiated by various factors on the released 40S

subunits. Such a cyclical process is crucial in maintaining the overall translation efficiency by supplying the translation machinery in a continuous manner.

Given the tremendous energy cost associated with protein synthesis, it is not surprising that global protein synthesis is generally suppressed under a diverse array of stress conditions.^{7,8} Indeed, many stress signaling pathways converge on key initiation factors, thereby limiting ribosome loading on mRNAs in response to stress.^{9,10} It is anticipated that once the cap-dependent translation initiation is inhibited, the unused ribosomal subunits accumulate inside cells. Despite the fact that some ribosomes are utilized for cap-independent mRNA translation,¹¹ very little is known about the behavior of free ribosomes in surplus. Under certain types of stress, some 40S ribosomal subunits are re-located into stress granules, serving as a stress response pathway.¹² When the free ribosome subunits are not engaged with any messengers, one imminent question is whether they re-associate into empty 80S ribosomes, maintain separate subunits, or actively disassemble into ribosomal proteins.

CONTACT Shu-Bing Qian  sq38@cornell.edu  301 Biotech, 526 Campus Road, Cornell University, Ithaca, NY 14853, USA.

[#]Present address: Program in Molecular Medicine, University of Massachusetts Medical School, Worcester, MA, USA.

 Supplemental material data for this article can be accessed on the publisher's website.

© 2016 Taylor & Francis

Sucrose gradient-based polysome profiling has been commonly used to separate free ribosomal subunits, monosomes, and polysomes.¹³ Given that actively translating mRNAs are often associated with multiple ribosomes, calculating the ratio of mRNA abundance in different fractions has been widely used as a measure of translational status under different growth conditions.¹⁴ Consistent with this notion, many stress conditions lead to evident polysome disassembly with a corresponding increase of 80S monosome.¹⁵ However, a substantial amount of ribosomes in the 80S fraction are empty as evidenced by the increased sensitivity to high salt treatment.¹⁶ It is unclear whether these empty ribosomes are simple byproducts during sample preparation or bear unappreciated biological information. Recent development of ribosome profiling technology, based on deep sequencing of ribosome-protected mRNA fragments (RPFs), enables monitoring of ribosome position and density at the genome-wide scale.¹⁷ However, ribosome profiling is not poised to capture empty ribosomes. Interestingly, ribosome profiling reveals pervasive footprints outside of protein-coding regions.¹⁸ The central dilemma that confronts researchers concerns whether the ribosome occupancy at the non-coding region represents true translation events or simple artifacts arisen from re-binding of free ribosomal subunits. It is thus crucial to exclude false positive ribosome footprints in the profiling analysis.

Here we report that empty ribosomes present in cell lysates can be evaluated based on their stable association with the elongation factor eEF2. Direct comparison of ribosome footprints between monosome and polysome fractions reveals distinct pattern of ribosome dynamics. In addition, the free ribosomal subunits minimally contributes to ribosome occupancy at the non-coding region. Our results not only offer a simple method to monitor ribosome availability, but potentially uncover additional layers of ribosome status needed to be considered in many translational profiling analyses.

Results

Differential distribution of elongation factors between monosome and polysome

Sucrose gradient-based sedimentation has been widely used for separation of 40S, 60S, 80S, and polysomes from cell extracts. Although the 80S

fraction contains empty ribosomes, the polysome is composed of actively translating ribosomes. eEF1A and eEF2 are mutually exclusive in binding to the ribosomal A-site and are expected to be present in the translating ribosomes.¹ To our surprise, in ribosome fractions obtained from HEK293 cells, both elongation factors were mainly located in the light fractions with few of these molecules detectable in the polysome fraction (Fig. 1A, left panel). A closer examination revealed that the 80S fraction contained more eEF2 than eEF1A, despite the fact that eEF1A is more abundant in cells.¹⁹ This result is consistent with the previous study in *S. cerevisiae* using quantitative mass spectrometry, in which EFT2 (the yeast homolog of eEF2) and TEF2 (the yeast homolog of eEF1A) were primarily co-purified with the monosome rather than the polysome.²⁰ In addition, more EFT2 was present in the monosome fraction of yeast cells.²⁰

It is possible that both elongation factors bind to the actively translating ribosomes with a fast kinetics and the association is not stable enough in the lysis buffer. To test this possibility, we conducted *in vivo* crosslinking before cell lysis using a Lomant's reagent DSP that is cleavable by reducing agent. Despite the improved recovery of eEF1A and eEF2 in the polysome fraction, both elongation factors were still highly concentrated in the light fractions (Fig. S1). In particular, the dominant presence of eEF2 in the monosome suggests that the ribosome in this fraction differs from the one undergoing active translation.

Prominent eEF2 association with ribosomes under proteotoxic stress

We next attempted to increase the monosome fraction of HEK293 cells by applying proteotoxic stress that potentially attenuates global protein synthesis.¹⁵ Pre-exposure of cells to a proline analog L-azetidine-2-carboxylic acid (AZC) and a proteasome inhibitor MG132 markedly reduced the polysome with a pronounced increase in the monosome (Fig. 1A, right panel). Interestingly, only eEF2, but not eEF1A, showed a corresponding increase in the monosome. This pattern was maintained after *in vivo* crosslinking using DSP (Fig. S1). To examine the ribosome-associated elongation factors in a more quantitative manner, we spin down all the ribosomes through a sucrose

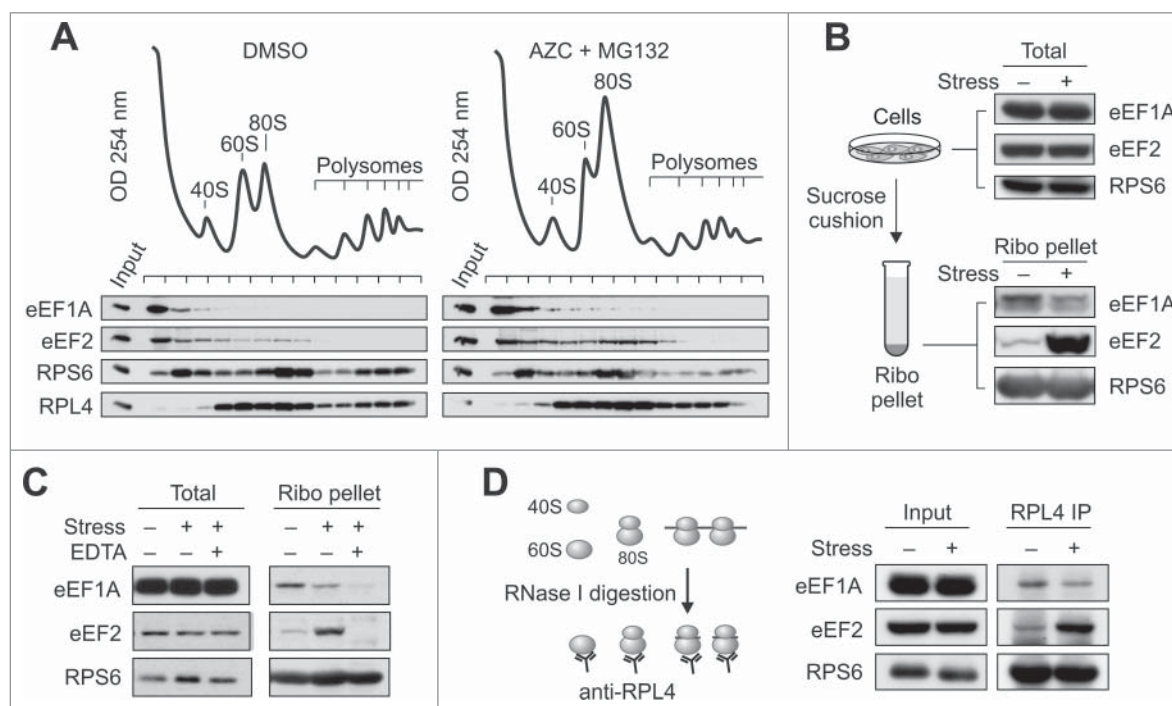


Figure 1. Differential association of elongation factors with ribosomes (A) HEK293 cells were pre-treated with 10 mM AZC and 20 μ M MG132 (right panel) or DMSO control (left panel) for 60 min followed by sucrose gradient sedimentation. Both the whole cell lysates (input) and ribosomes fractions were immunoblotted using antibodies indicated. (B) Sucrose cushion analysis of ribosome-associated elongation factors in HEK293 cells with or without proteotoxic stress. Both the whole cell lysates (total) and ribosome pellets were immunoblotted using antibodies indicated. (C) Sucrose cushion analysis of ribosome-associated elongation factors in samples as (B) in the presence of absence of 40 μ M EDTA. (D) Ribosome immunoprecipitation analysis of ribosome-associated elongation factors. Whole cell lysates as (B) were treated with RNase I to convert polysome into monosome followed by anti-RPL4 immunoprecipitation.

cushion (Fig. 1B). For cells under proteotoxic stress, eEF1A showed a minor but obvious reduction in the ribosome pellet. Remarkably, eEF2 exhibited a striking accumulation in the same ribosome pellet. The eEF2 co-sedimentation is a result of association with the 80S ribosome because EDTA treatment greatly abolished the accumulation of both elongation factors (Fig. 1C). To exclude the non-specific eEF2 association in the ribosome pellet, we purified ribosomes using affinity immunoprecipitation (IP) from cell lysates treated with RNase I to convert all ribosomes into monosome (Fig. 1D). Consistent with the sucrose cushion result, less eEF1A but more eEF2 molecules were precipitated from stressed cells by an antibody against RPL4, a core ribosomal protein. This result suggests that eEF2 preferentially associates with non-translating ribosomes.

eEF2 preferentially associates with empty ribosomes

We previously demonstrated that proteotoxic stress caused an early ribosomal pausing on mRNAs.¹⁵ It is

unclear whether eEF2 preferentially binds to the paused ribosome or the empty ribosome without mRNA. To distinguish these 2 possibilities, we conducted nascent chain IP to collect specific mRNA-engaged ribosomes followed by detection of elongation factors (Fig. S2). Consistent with the early pausing,¹⁵ more ribosomes were associated with the nascent chain in the presence of AZC and MG132. However, proteotoxic stress did not lead to any accumulation of eEF2 in the purified ribosomes synthesizing Flag-GFP. This result further suggests that eEF2 preferentially associates with empty ribosomes without mRNA engagement.

Many stress conditions lead to an increased monosome fraction as a result of repression in global protein synthesis.²¹ If eEF2 preferentially binds to empty ribosomes, then different types of stress would lead to the same consequence. Indeed, oxidative stress by sodium arsenite treatment or heat shock stress potentially induced eEF2 accumulation in the ribosome pellet (Fig. 2A). In contrast, eEF1A showed a corresponding decrease in the

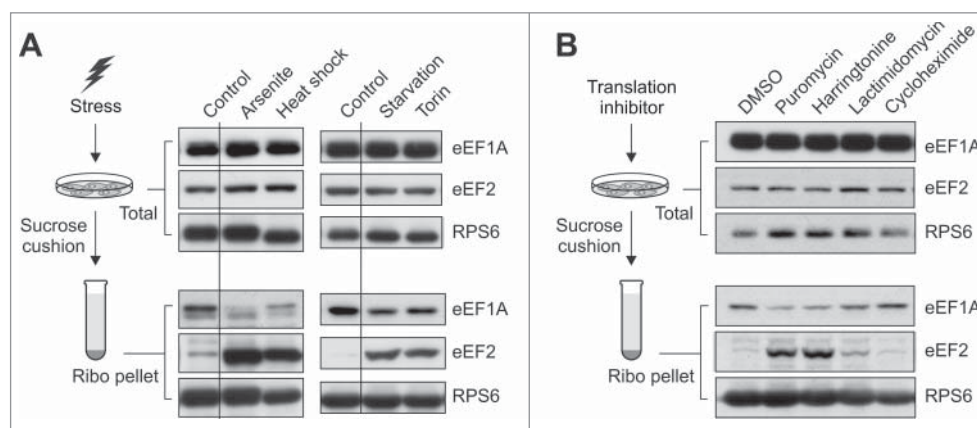


Figure 2. eEF2 stably associates with empty ribosomes. (A) Sucrose cushion analysis of ribosome-associated elongation factors in HEK293 cells under various stress conditions, including arsenite (0.5 mM for 60 min), heat shock (43°C for 60 min), amino acid starvation (60 min), or torin (250 nM for 60 min). Both the whole cell lysates (total) and ribosome pellets were immunoblotted using antibodies indicated. Black line indicates that some intervening lanes were removed from the same gel image. (B) Sucrose cushion analysis of ribosome-associated elongation factors in HEK293 cells under various stress conditions, including puromycin (100 μ M for 60 min), harringtonine (2 μ g/mL for 60 min), lactimidomycin (50 μ M for 60 min), or cycloheximide (100 μ M for 60 min). Both the whole cell lysates (total) and ribosome pellets were immunoblotted using antibodies indicated.

same samples. To substantiate the finding further, we suppressed cap-dependent translation initiation by applying amino acid starvation or treating cells with Torin, a potent inhibitor of mammalian target of rapamycin complex I (mTORC1).²² Both conditions unequivocally led to eEF2 build-up in the ribosome pellet with a corresponding decrease of eEF1A (Fig. 2A).

To definitively demonstrate that eEF2 associates with empty ribosomes only, we took advantage of a panel of translation inhibitors. Puromycin acts as a tRNA analog, releases the nascent chain from the ribosome P-site, and dissociates the ribosome into separate subunits.²³ As expected, puromycin treatment completely disassembled the polysome with a dramatic increase of the monosome fraction (Fig. S3). Similar to many stress conditions aforementioned, puromycin treatment resulted in a prominent accumulation of eEF2 in the ribosome pellet (Fig. 2B). The elongation inhibitor cycloheximide is known to stabilize the polysome by immobilizing ribosomes on the mRNA, thereby limiting the amount of free ribosomes. As a result, few eEF2 was detectable in the ribosome pellet from cells after cycloheximide treatment. Notably, the inverse correlation between eEF2 and eEF1A was evident in these ribosome pellets. Thus, the relative ratio of these 2 elongation factors can be used to evaluate the ribosome status in a quantitative manner.

We next tested 2 additional translation inhibitors known to immobilize the initiating ribosome. Harringtonine binds to the free 60S ribosome subunit and prevents the first peptide bond formation upon the 80S assembly.²⁴ Despite the potential enrichment of ribosomes at the initiation sites,²⁵ a substantial amount of eEF2 was accumulated in the ribosome pellet (Fig. 2B). This result suggests that a large portion of ribosomes cannot undergo initiation in the presence of harringtonine. Alternatively, the harringtonine-immobilized ribosomes are not stable. Unlike harringtonine, lactimidomycin preferentially acts on the initiating ribosomes by binding to the empty E-site.²⁶ In cells treated with lactimidomycin, fewer eEF2 molecules were recovered from the ribosome pellet in comparison to harringtonine treatment (Fig. 2B). Although lactimidomycin permits new rounds of initiation that uses free ribosomes,²⁷ we cannot exclude the possibility that the presence of this compound may prevent stable eEF2 binding to the empty ribosome.

Examining empty ribosomes by ribosome profiling

Given the increasing popularity of ribosome profiling in studying translational regulation,²⁸ we wonder whether the presence of empty ribosomes might perturb high-throughput sequencing of ribosome footprints. We reason that the empty 80S ribosomes are likely formed by simple re-association of free 40S

and 60S subunits in the lysis buffer. The lack of mRNA permits stable eEF2 binding. However, such random association of ribosomal subunits could lead to promiscuous binding to various RNA species present in the lysates. These non-translating ribosomes could leave non-specific footprints that are indistinguishable from true footprints. These false positives, if present, are likely to be amplified under stress conditions because of the large amount of free ribosomes after severe translational inhibition.

Since the majority of empty ribosomes comigrate with the 80S monosome on the sucrose gradient, we separated the 80S monosome from the total fractions using HEK293 lysates (Fig. 3A). Both samples were then subject to RNase I digestion followed by library construction. We omitted the rRNA-depletion step so we could count total reads mapped to mRNA and rRNA respectively.

Empty ribosomes are expected to give rise to reads derived from rRNA only, but not mRNA. Indeed, the monosome showed a 4-fold lower mRNA/rRNA ratio in comparison to the total fractions (Fig. 3B and Table 1). It is possible that the increased rRNA reads in the monosome were partially derived from the contaminated free 40S and 60S subunits. By taking into account their maximal OD254 value, still approximately half of the monosomes are not associated with any mRNA fragments. Despite the increased proportion of rRNA reads in the monosome fraction, individual rRNA read maps were comparable between the 2 samples (Fig. S4). The highly clustered rRNA read pattern is consistent with the structure of mammalian ribosomes with many rRNA segments exposed outside.²⁹ The similar rRNA read pattern in all the ribosome fractions suggests that the empty 80S

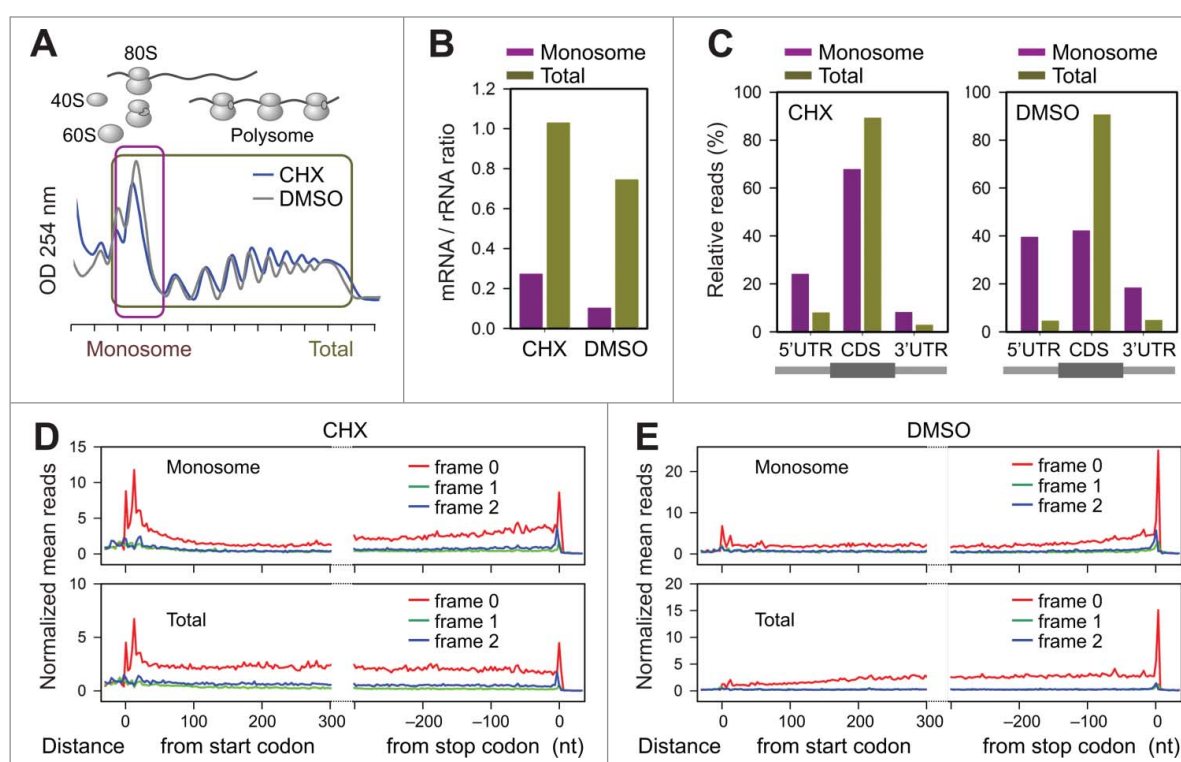


Figure 3. Examine empty ribosomes by ribosome profiling. (A) Sucrose gradient sedimentation of whole cell lysates from HEK293 cells in the absence (DMSO, gray line) or presence of 100 μ M cycloheximide (CHX, blue line). Both the monosome (purple box) and the total fraction (dark yellow box) were collected for ribosome profiling. (B) The monosome and total ribosomes fractions shown in (A) were subject to separate ribosome profiling. Relative ratio of reads mapped to mRNA and rRNA was used to evaluate the amount of empty ribosomes in the monosome. (C) Fractions of reads mapped to different regions of mRNA were quantified for the monosome (left panel) and the total fractions (right panel) as shown in (A). (D) Metagene analysis of ribosome-protected fragments derived from the monosome (top panel) or the total fraction (bottom panel) in the presence of 100 μ M cycloheximide. Normalized reads are averaged across the transcriptome, aligned at either their start or stop codons. Different reading frames are color coded. (E) Metagene analysis of ribosome-protected fragments derived from the monosome (top panel) or the total fraction (bottom panel) in the absence of 100 μ M cycloheximide.

ribosome resembles the translating ribosomes in terms of the overall conformation.

Interpreting monosome in the presence of empty ribosomes

With the presence of large quantity of empty ribosomes, the increased rRNA reads would reduce the mRNA read depth in the monosome. However, we are more concerned whether some of these inert ribosomes would randomly bind to mRNA species. This concern arises from traditional *in vitro* translation experiments, in which purified ribosome subunits readily bind to the poly(U) template independent of initiation factors.³⁰ If random binding occurs in the current system, the resultant false footprints would increase the read density in the non-coding region and decrease the 3-nt periodicity (phasing) in the coding region. Compared to the reads obtained from total fractions, monosome-derived footprints showed higher occupancy in the non-coding region, in particular 5'UTR (Fig. 3C). However, the 5'UTR ribosome occupancy could result from uORF translation, which is over-represented in the monosome because of the linear scanning process of initiating ribosomes.³¹ Notably, both the monosome and the total fractions maintained a dominant single reading frame (Fig. S5A), arguing against the random association of free ribosomal subunits on transcripts.

Interestingly, the monosome demonstrated a distinct pattern of read distribution in comparison to the total fractions. Unlike the polysome that exhibits uniform distribution of reads along the CDS, the monosome showed fewer reads in the middle region of the CDS (Fig. 3D). This result is consistent with the notion that ribosome moves relatively slower shortly after initiation and before termination.³² In polysomes, however, prolonged pausing of the leading ribosome often leads to stacking of the following ribosomes, causing increased ribosome density at multiple positions. Without the influence of neighboring ribosomes, the monosome fraction may be more valuable than the polysome in revealing elongation speed and assessing decoding kinetics.^{33,34}

To further exclude the possibility of non-specific ribosome binding, we sought to increase the amount of free ribosomal subunits in cells. Many stress conditions lead to increased free ribosomes as a result of translation inhibition (Fig. 2A). However, non-

canonical translation could also be induced under these conditions and it is difficult to distinguish true uORF translation from non-specific footprints. We therefore chose to increase the amount of free ribosomes without changing the growth condition. Ribosome profiling typically uses translation inhibitors like cycloheximide to immobilize ribosomes on transcripts.³⁵ In the absence of translation inhibitors, some ribosomes are expected to run off. Indeed, without cycloheximide treatment, the polysome was slightly reduced with a concomitant increase of monosome (Fig. 3A). Consistent with the runoff process, a substantial amount of reads were migrated toward the end of the CDS, including the stop codon (Fig. 3E). Further supporting the formation of more empty ribosomes in the absence of cycloheximide, a lower mRNA/rRNA read ratio was evident in all ribosome fractions (Fig. 3B).

Among the reads mapped to transcriptome in the absence of cycloheximide, the monosome showed a drastic reduction of CDS occupancy relative to the cycloheximide-treated sample (Fig. 3C, right panel). Despite the lower ribosome density in the absence of cycloheximide, the monosome maintained the strong 3-nt periodicity in the CDS region (Fig. S5B). Therefore, free ribosomal subunits do not undergo non-specific mRNA binding, at least to the coding region. Notably, the apparent increase of read density in both 5'UTR and 3'UTR regions is not an absolute value. When the total read amount is normalized for the monosome, the amount of 3'UTR read density was maintained at the similar levels in the presence or absence of cycloheximide (Fig. S6A). This is consistent with the notion that the 3'UTR occupancy likely represents background signals, presumably due to the presence of RNA-binding protein (RNPs) co-migrating with ribosomes¹⁸. Supporting this notion, reads mapped to 3'UTR showed neither dominant reading frames nor typical read length distribution (Fig. S6B and C). Since no additional reads were detected above the background signals of 3'UTR, the increased free ribosomes in the absence of cycloheximide does not contribute to ribosome occupancy outside of the coding region.

Discussion

It has been estimated that a typical mammalian cell contains about 3,000,000 ribosomes. However, the

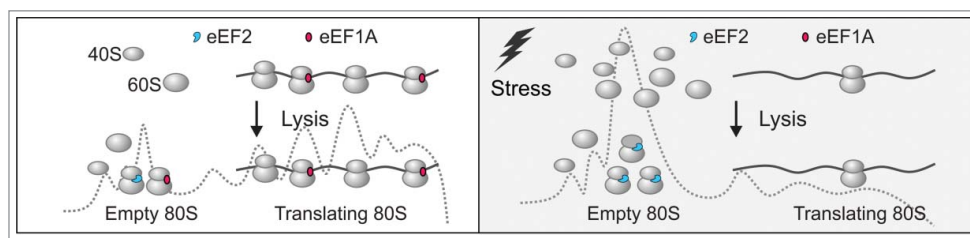


Figure 4. Multiple ribosome status in translational profiling. A schematic model depicting different ribosome status in cells. Under the normal growth condition (left panel), multiple ribosomes are loaded onto single transcripts, leaving fewer ribosomal subunits and empty ribosomes. Under stress conditions (right panel), global repression of translation leads to accumulation of free ribosomal subunits that tend to form empty ribosomes stably associated with eEF2.

quantity of total mRNAs is less than 300,000 per cell.³⁶ Although polysomes are common in proliferating cells, not all the transcripts are equally used for active translation.³⁷ It is therefore not surprising to find many empty ribosomes in cells even under the normal growth condition. Upon stress, global translation repression leads to more free ribosomes that potentially influence the intracellular milieu. However, the presence of large quantity of non-translating ribosomes is virtually ignored in most translational profiling analysis. The ability to quantify empty ribosomes at any given cellular stage will aid in our understanding of translational regulation.

Despite long appreciation of the spare ribosomes in cells, no simple way is available to distinguish empty ribosomes from translating ribosomes. A commonly used approach relies on high salt sensitivity of the 80S ribosome fraction separated on a sucrose gradient.¹⁶ Although informative, the salt sensitivity can be influenced by many confounding factors in the buffer system and does not offer reliable quantification. We found that empty ribosomes preferentially bind to eEF2, an elongation factor that is essential for translocation. Surprisingly, eEF2 is largely absent in polysomes captured by sucrose gradient sedimentation, which is consistent with the transient nature of the translocation process (within milliseconds).³⁸ In prokaryotes, EF-G can be trapped on the translating ribosome only by using nonhydrolyzable analogs of GTP as demonstrated in recent crystal structures of 70S ribosomes.³⁹⁻⁴¹ Interestingly, mammalian ribosomes prepared using high salt led to constant presence of eEF2, but not other translation factors.^{29,42,43} Our results clearly indicate that eEF2 stably binds to empty ribosomes, although we do not know whether the binding occurs inside cells or in the lysis buffer.

Regardless, it is clear that the level of ribosome-bound eEF2 is proportional to the amount of free ribosomes. This feature offers a sensitive means to evaluate ribosome availability under various stress conditions (Fig. 4). In addition, it provides unique aspects of ribosome status in the presence of different translation inhibitors.

Classic translation assays using a reconstituted *in vitro* system demonstrated that purified ribosomal subunits can associate with poly(U) to direct the synthesis of polyphenylalanine in the absence of initiation factors.⁴⁴ The large quantity of mRNA-free ribosomes present in the monosome raises an imminent question about the possibility of random ribosome binding to transcripts. This issue is particularly important in deep sequencing-based ribosome profiling.²⁸ Indeed, this approach reveals pervasive ribosome occupancy outside of annotated protein-coding regions, including 5'UTRs as well as long intergenic noncoding RNAs (lincRNAs).¹⁸ Although mass spectrometry experiments confirmed the existence of some peptides derived from these non-coding regions,^{45,46} the question lingers whether all of these ribosomes are truly undergoing active translation. A growing body of evidence suggests that ribosome engagement has impacts beyond the production of polypeptides. However, it is crucial to exclude false positive ribosome footprints in the profiling analysis. Those non-specific ribosome binding include, but not limited to, random association of free ribosomal subunits and constant binding of RNPs co-sedimented with ribosome. We provide experimental evidence that free subunits undergo minimal non-specific association on transcripts. This result is consistent with the recent report that mixing mammalian and yeast

cell lysates did not generate “cross-over” footprints, although the amount of free ribosomes was unclear.¹⁸

The significance of understanding different ribosome status is also reflected in recently established initiating ribosome profiling,²⁷ which has proven to be powerful in uncovering hidden coding potential of transcriptomes. These approaches often rely on elongating ribosome runoff that generates an enormous amount of free ribosomes highly enriched in the monosome.^{25,27,47,48} Given the unique feature of eEF2 binding, we anticipate that it is now possible to deplete empty ribosomes from the monosome by using anti-eEF2 antibodies. We are currently testing this possibility as part of the continuous optimization of existing profiling protocols. Taken together, our results provide a useful platform for further improvement of translational profiling, experimentally and analytically.

Materials and methods

Cells and reagents

HEK293 cells were maintained in Dulbecco's Modified Eagle's Medium (DMEM) with 10% fetal bovine serum (FBS). L-azetidine-2-carboxylic acid (AZC), Z-Leu-Leu-Leu-al (MG132), sodium arsenite (NaAsO₂), cycloheximide (CHX), Ethylenediaminetetraacetic acid (EDTA), puromycin and secondary antibodies were purchased from Sigma. Torin (Tocris bioscience) and harringtonine (LKT Laboratories) were also purchased. Lactimidomycin was generously provided by Dr. Ben Shen (Scripps, Florida). Anti-rpS6 (Cell signaling), anti-eEF2 (Cell signaling), anti-eEF1A (Millipore), and anti-rpL4 (ProteinTech) antibodies were acquired. Dithiobis[succinimidyl propionate]; (DSP) and sucrose were from Thermo Fisher Scientific.

Ribosome separation on sucrose gradient

Polysome buffer (pH 7.4, 10 mM HEPES, 100 mM KCl, 5 mM MgCl₂) was used to prepare all sucrose solutions. Sucrose density gradients (15%–45% w/v) were freshly made in SW41 ultracentrifuge tubes (Beckman) using a Gradient Master (BioComp Instruments) according to manufacturer's instructions. Cells were pre-treated with 100 µg/ml cycloheximide for 3 min at 37°C to stabilize ribosomes on mRNAs followed by washing using ice-cold PBS containing 100 µg/ml cycloheximide. Cells were then lysed on ice

by scraping extensively in polysome lysis buffer (pH 7.4, 10 mM HEPES, 100 mM KCl, 5 mM MgCl₂, 100 µg/ml cycloheximide and 2% Triton X-100). Cell debris were removed by centrifugation at 14,000 rpm for 10 min at 4°C. 600 µl of supernatant was loaded onto sucrose gradients followed by centrifugation for 150 min at 32,000 rpm 4°C in a SW41 rotor. Separated samples were fractionated at 1.5 ml / min through a fractionation system (Isco) that continually monitored OD₂₅₄ values. Fractions were collected with 0.5 min interval. For DMSO samples, CHX in all buffers was replaced with equal amount of DMSO. For puromycin treatment, 100 µM puromycin was added during the pre-treatment instead of CHX.

For the DSP crosslinking, medium was aspirated out and cells were washed once with PBS (RT) to remove free amino acid residuals as much as possible. Crosslinking was performed with 2.5 mM DSP in PBS (RT) at RT for 1 min and quenched with 50 mM Tris (pH7.0) at RT for 1 min. After the aspiration of supernatants, cells were washed with ice-cold PBS (100 µg/ml CHX) once and lysed with polysome lysis buffer. Before immunoblotting, crosslinking was reversed by incubating samples in sample buffer (with 100 mM DTT) at 37°C for 30 min.

Ribosome pelleting on sucrose cushion

300 µl cleared lysate was laid on top of 900 µl 1M sucrose in Beckman centrifugation tubes. Ribosomes were pelleted by centrifugation at 78,000 rpm for 120 min at 4°C using a Beckman TLA-110 rotor. After removing the supernatant, ribosome pellets were rinsed with polysome buffer once and resuspended in sample buffer (50 mM Tris-HCl, pH 6.8, 100 mM dithiothreitol, 2% SDS, 0.1% bromophenol blue, 10% glycerol) for immunoblotting.

Immunoprecipitation and immunoblotting

Cells were pre-treated with 100 µg/ml cycloheximide at 37°C for 3 mins to stabilize ribosome complexes and washed once with ice-cold PBS plus 100 µg/ml CHX. Cells were then scraped extensively in polysome lysis buffer supplemented with EDTA-free cocktail protease inhibitor (Roche). After clearance by centrifugation for 10 min at 14,000 rpm at 4°C, the supernatant was collected and incubated with 200 U RNaseI (Ambion) and anti-RpL4 antibody at 4°C for 1 h. After that, protein A beads previously equilibrated

with polysome lysis buffer were incubated with the mixture at 4°C for 1 h. Beads were washed for 3 times with polysome lysis buffer and associated proteins were eluted by heating at 95°C for 10 min in the sample buffer. For immunoprecipitation of ribosome-associated nascent chains, lysate was incubated with anti-Flag M2 affinity gel (Sigma) at 4°C for 1 h without RNaseI digestion.

For immunoblotting, protein samples were resolved on SDS-PAGE and then transferred to Immobilon-P membranes (Millipore). After blocking for 1 hour in TBS containing 5% blotting milk, membranes were incubated with primary antibodies at 4°C overnight. After incubation with horseradish peroxidase-coupled secondary antibodies, immunoblots were developed using enhanced chemiluminescence (GE Healthcare). Densitometry is used to quantify the immunoblotting bands. In brief, specific bands with equal surface areas were selected using ImageQuant followed by gray scale measurement. A blank areas was also include as background levels. Relative ratio was calculated using control as 1.

Ribosome profiling

Sucrose gradient fractions corresponding to only monosome or monosome with polysome were pooled and a 200 μ l aliquot was digested with 200U *E. coli* RNase I (Ambion) at 4°C for 1 h. Total RNAs were extracted using Trizol reagent (Invitrogen). Subsequently, RNA molecules were dephosphorylated by 20U T4 polynucleotide kinase (NEB) in the presence of 10 U SUPERase (Ambion) at 37°C for 1 hour. The enzyme was heat-inactivated for 20 min at 65°C. The products were then separated on a Novex denaturing 15% polyacrylamide TBE-urea gel (Invitrogen). Gel bands corresponding to 28-30 nt RNA molecules were excised and physically disrupted by centrifugation through the holes of the tube. Resulting gel debris was soaked overnight in the RNA gel elution buffer (300 mM NaOAc pH 5.5, 1 mM EDTA, 0.1 U/ μ l SUPERase_In) to recover RNA fragments. The gel debris was filtered out with a Spin-X column (Corning) and RNA was finally purified using ethanol precipitation.

The cDNA library construction was described²⁷. In brief, Poly-A tails were added to the purified RNA fragments by *E. coli* poly-(A) polymerase (NEB) with 1 mM ATP in the presence of 0.75 U/ μ L

SUPERase_In at 37°C for 45 min. The tailed RNA molecules were reverse transcribed to generate the first strand cDNA using SuperScript III (Invitrogen) and following oligos containing barcodes:

MCA02, 5'-pCAGATCGTCGGACTGTAGAACTCT
 Ø CAAGCAGAAGACGGCATAACGATT TTTT TTTT TTT
 TTTT TTTT TVN-3';
 LGT03, 5'-pGTGATCGTCGGACTGTAGAACTCT Ø
 CAAGCAGAAGACGGCATAACGATT T
 TTTT TTTT TTTT TTTT TTTT TVN-3';
 YAG04, 5'-pAGGATCGTCGGACTGTAGAACTCT Ø
 CAAGCAGAAGACGGCATAACGATT TTTT TTTT TTTT
 TTTT TTTT TVN-3';
 HTC05, 5'-pTCGATCGTCGGACTGTAGAACTC
 T Ø CAAGCAGAAGACGGCATAACGATT
 TTTT TTTT TTTT TTTT TTTT TVN-3'

Reverse transcription products were resolved on a 10% polyacrylamide TBE-urea gel as described above. The expected 92 nt band of first strand cDNA was excised and recovered as above using DNA gel elution buffer (300 mM NaCl, 1 mM EDTA). Purified first strand cDNA was then circularized by 100U CircLi-gase II (Epicentre) following manufacturer's instructions. The resulting circular single strand DNA was purified using ethanol precipitation and re-linearized by 7.5 U APE 1 in 1 X buffer 4 (NEB) at 37°C for 1 h. The products were resolved on a Novex 10% polyacrylamide TBE-urea gel (Invitrogen) as described above. The expected 92 nt band was then excised and recovered. Finally, single-stranded template was amplified by PCR using the Phusion High-Fidelity enzyme (NEB) according to the manufacturer's instructions. The primers qNTI200 (5'-CAAGCA-GAAGACGGCATA-3') and qNTI201 (5'-AATGA-TACGGCGACCACCG ACAGGTTTCAGAGTTCTA-CAGTCCGACG-3') were used to create DNA library suitable for sequencing. The PCR reaction contains 1× HF buffer, 0.2 mM dNTP, 0.5 μ M primers, 0.5U Phusion polymerase. PCR was carried out with an initial 30 s denaturation at 98°C, followed by 12 cycles of 10 s denaturation at 98°C, 20 s annealing at 60°C, and 10 s extension at 72°C. PCR products were separated on a non-denaturing 8% polyacrylamide TBE gel as described above. Expected 120 bp band was excised and recovered as described above. After quantification by Agilent BioAnalyzer DNA 1000 assay, equal amount of barcoded samples were pooled into one sample. 3 ~ 5 pmol mixed DNA samples were

Table 1. Statistics of ribosome profiling.

Sample	Total	Trimmed 25-35	Mapped to rRNA	Mapped to mRNA
DMSO_Mono	21492787	15589353	6895309	698,779
CHX_Mono	22612056	17822729	7635030	2,071,271
DMSO_Total	22733871	11162662	4659077	3,461,257
CHX_Total	23620446	17601268	6534415	6,719,868

typically used for cluster generation followed by sequencing using sequencing primer 5'-CGA-CAGGTTTCAGAGTTC TACAGTCCGACGATC-3' (HiSEQ2000, Cornell University Life Sciences Core Laboratories Center).

Data analysis

The next-generation sequencing data of ribosome footprints was processed and analyzed using a collection of custom Perl scripts. The barcoded multiplex sequencing output files were separated into individual sample datasets according to the first 2-nucleotide barcodes. To remove adaptor sequences, 7 nucleotides were cut from the 3' end of each 50-nt-long Illumina sequence read, and the 3' polyA tails were identified and removed allowing 1 mismatch. The high quality reads of length ranging from 25 to 35 nt were then retained while other reads were excluded from the downstream analysis. A set of longest mRNA transcripts and associated CDS annotation were compiled from RefSeq Human transcriptome reference (downloaded from NCBI on 09-17-2012) by comparing different mRNA isoforms of the same gene on CDS length (if CDS lengths are the same, 5' UTR lengths are compared). The trimmed reads were first aligned to human rRNA sequences and unmapped reads were mapped to the representative longest mRNAs by Bowtie-0.12.3. One mismatch was allowed in all mappings; in cases of multiple mapping, mismatched positions were not used if a perfect match existed. Reads mapped more than 100 times were discarded to remove poly-A-derived reads. Finally, reads were counted at every position of individual transcripts by using the 13th nucleotide of the read for the P-site position. For the read aggregation plot, only mRNAs with at least 30nt UTR, 300nt CDS, and 50 mapped reads in all samples were included. The number of reads aligned to each position of individual mRNA was first normalized by the total number of reads recovered from the same mRNA. The read counts

were then averaged across all mRNAs for each position relative to the annotated start or stop codon.

Disclosure of potential conflicts of interest

No potential conflicts of interest were disclosed.

Acknowledgements

We'd like to thank Qian lab members for helpful discussion. We also thank Cornell University Life Sciences Core Laboratory Center for performing deep sequencing.

Funding

This work was supported by grants to S.-B.Q. from US National Institutes of Health (R01AG042400), and US Department of Defense (W81XWH-14-1-0068).

References

- [1] Jackson RJ, Hellen CU, Pestova TV. The mechanism of eukaryotic translation initiation and principles of its regulation. *Nat Rev Mol Cell Biol* 2010; 11:113-27; PMID:20094052; <http://dx.doi.org/10.1038/nrm2838>
- [2] Sonenberg N, Hinnebusch AG. New modes of translational control in development, behavior, and disease. *Mol Cell* 2007; 28:721-9; PMID:18082597; <http://dx.doi.org/10.1016/j.molcel.2007.11.018>
- [3] Aitken CE, Lorsch JR. A mechanistic overview of translation initiation in eukaryotes. *Nat Struct Mol Biol* 2012; 19:568-76; PMID:22664984; <http://dx.doi.org/10.1038/nsmb.2303>
- [4] Hinnebusch AG. The scanning mechanism of eukaryotic translation initiation. *Annu Rev Biochem* 2014; 83:779-812; PMID:24499181; <http://dx.doi.org/10.1146/annurev-biochem-060713-035802>
- [5] Kong J, Lasko P. Translational control in cellular and developmental processes. *Nat Rev Genet* 2012; 13:383-94; PMID:22568971; <http://dx.doi.org/10.1038/nrg3184>
- [6] Jackson RJ, Hellen CU, Pestova TV. Termination and post-termination events in eukaryotic translation. *Adv Protein Chem Struct Biol* 2012; 86:45-93; PMID:22243581; <http://dx.doi.org/10.1016/B978-0-12-386497-0.00002-5>
- [7] Holcik M, Sonenberg N. Translational control in stress and apoptosis. *Nat Rev Mol Cell Biol* 2005; 6:318-27; PMID:15803138; <http://dx.doi.org/10.1038/nrm1618>

- [8] Liu B, Qian SB. Translational reprogramming in cellular stress response. *Wiley Interdiscip Rev RNA* 2014; 5 (3):301-15; PMID: 24375939; <http://dx.doi.org/10.1002/wrna.1212>
- [9] Ma XM, Blenis J. Molecular mechanisms of mTOR-mediated translational control. *Nat Rev Mol Cell Biol* 2009; 10:307-18; PMID:19339977; <http://dx.doi.org/10.1038/nrm2672>
- [10] Harding HP, Calton M, Urano F, Novoa I, Ron D. Transcriptional and translational control in the Mammalian unfolded protein response. *Annu Rev Cell Dev Biol* 2002; 18:575-99; PMID:12142265; <http://dx.doi.org/10.1146/annurev.cellbio.18.011402.160624>
- [11] Hellen CU, Sarnow P. Internal ribosome entry sites in eukaryotic mRNA molecules. *Genes Dev* 2001; 15:1593-612; PMID:11445534; <http://dx.doi.org/10.1101/gad.891101>
- [12] Buchan JR, Parker R. Eukaryotic stress granules: the ins and outs of translation. *Mol Cell* 2009; 36:932-41; PMID:20064460; <http://dx.doi.org/10.1016/j.molcel.2009.11.020>
- [13] Masek T, Valasek L, Pospisek M. Polysome analysis and RNA purification from sucrose gradients. *Methods Mol Biol* 2011; 703:293-309; PMID:21125498; http://dx.doi.org/10.1007/978-1-59745-248-9_20
- [14] Arava Y, Wang Y, Storey JD, Liu CL, Brown PO, Herschlag D. Genome-wide analysis of mRNA translation profiles in *Saccharomyces cerevisiae*. *Proc Natl Acad Sci U S A* 2003; 100:3889-94; PMID:12660367; <http://dx.doi.org/10.1073/pnas.0635171100>
- [15] Liu B, Han Y, Qian SB. Cotranslational response to proteotoxic stress by elongation pausing of ribosomes. *Mol Cell* 2013; 49:453-63; PMID:23290916; <http://dx.doi.org/10.1016/j.molcel.2012.12.001>
- [16] Martin TE, Hartwell LH. Resistance of active yeast ribosomes to dissociation by KCl. *J Biol Chem* 1970; 245:1504-6; PMID:5442831
- [17] Ingolia NT, Ghaemmaghami S, Newman JR, Weissman JS. Genome-wide analysis in vivo of translation with nucleotide resolution using ribosome profiling. *Science* 2009; 324:218-23; PMID:19213877; <http://dx.doi.org/10.1126/science.1168978>
- [18] Ingolia NT, Brar GA, Stern-Ginossar N, Harris MS, Talhouarne GJ, Jackson SE, Wills MR, Weissman JS. Ribosome profiling reveals pervasive translation outside of annotated protein-coding genes. *Cell Rep* 2014; 8:1365-79; PMID:25159147; <http://dx.doi.org/10.1016/j.celrep.2014.07.045>
- [19] Mateyak MK, Kinzy TG. eEF1A: thinking outside the ribosome. *J Biol Chem* 2010; 285:21209-13; PMID:20444696; <http://dx.doi.org/10.1074/jbc.R110.113795>
- [20] Fleischer TC, Weaver CM, McAfee KJ, Jennings JL, Link AJ. Systematic identification and functional screens of uncharacterized proteins associated with eukaryotic ribosomal complexes. *Genes Dev* 2006; 20:1294-307; PMID:16702403; <http://dx.doi.org/10.1101/gad.1422006>
- [21] Sonenberg N, Hinnebusch AG. Regulation of translation initiation in eukaryotes: mechanisms and biological targets. *Cell* 2009; 136:731-45; PMID:19239892; <http://dx.doi.org/10.1016/j.cell.2009.01.042>
- [22] Thoreen CC, Chantranupong L, Keys HR, Wang T, Gray NS, Sabatini DM. A unifying model for mTORC1-mediated regulation of mRNA translation. *Nature* 2012; 485:109-13; PMID:22552098; <http://dx.doi.org/10.1038/nature11083>
- [23] Blobel G, Sabatini D. Dissociation of mammalian polyribosomes into subunits by puromycin. *Proc Natl Acad Sci U S A* 1971; 68:390-4; PMID:5277091; <http://dx.doi.org/10.1073/pnas.68.2.390>
- [24] Fresno M, Jimenez A, Vazquez D. Inhibition of translation in eukaryotic systems by harringtonine. *Eur J Biochem* 1977; 72:323-30; PMID:319998; <http://dx.doi.org/10.1111/j.1432-1033.1977.tb11256.x>
- [25] Ingolia NT, Lareau LF, Weissman JS. Ribosome profiling of mouse embryonic stem cells reveals the complexity and dynamics of mammalian proteomes. *Cell* 2011; 147:789-802; PMID:22056041; <http://dx.doi.org/10.1016/j.cell.2011.10.002>
- [26] Schneider-Poetsch T, Ju J, Eyler DE, Dang Y, Bhat S, Merrick WC, Green R, Shen B, Liu JO. Inhibition of eukaryotic translation elongation by cycloheximide and lactimidomycin. *Nat Chem Biol* 2010; 6:209-17; PMID:20118940; <http://dx.doi.org/10.1038/nchembio.304>
- [27] Lee S, Liu B, Huang SX, Shen B, Qian SB. Global mapping of translation initiation sites in mammalian cells at single-nucleotide resolution. *Proc Natl Acad Sci U S A* 2012; 109:E2424-32; PMID:22927429; <http://dx.doi.org/10.1073/pnas.1207846109>
- [28] Ingolia NT. Ribosome profiling: new views of translation, from single codons to genome scale. *Nat Rev Genet* 2014; 15:205-13; PMID:24468696; <http://dx.doi.org/10.1038/nrg3645>
- [29] Anger AM, Armache JP, Berninghausen O, Habeck M, Subklewe M, Wilson DN, Beckmann R. Structures of the human and *Drosophila* 80S ribosome. *Nature* 2013; 497:80-5; PMID:23636399; <http://dx.doi.org/10.1038/nature12104>
- [30] Arlinghaus R, Shaefer J, Schweet R. Mechanism of Peptide Bond Formation in Polypeptide Synthesis. *Proc Natl Acad Sci U S A* 1964; 51:1291-9; PMID:14215654; <http://dx.doi.org/10.1073/pnas.51.6.1291>
- [31] Kozak M. Pushing the limits of the scanning mechanism for initiation of translation. *Gene* 2002; 299:1-34; PMID:12459250; [http://dx.doi.org/10.1016/S0378-1119\(02\)01056-9](http://dx.doi.org/10.1016/S0378-1119(02)01056-9)
- [32] Petrov A, Kornberg G, O'Leary S, Tsai A, Uemura S, Puglisi JD. Dynamics of the translational machinery. *Curr Opin Struct Biol* 2011; 21:137-45; PMID:21256733; <http://dx.doi.org/10.1016/j.sbi.2010.11.007>
- [33] Plotkin JB, Kudla G. Synonymous but not the same: the causes and consequences of codon bias. *Nat Rev Genet* 2011; 12:32-42; PMID:21102527; <http://dx.doi.org/10.1038/nrg2899>

- [34] Fredrick K, Ibba M. How the sequence of a gene can tune its translation. *Cell* 2010; 141:227-9; PMID:20403320; <http://dx.doi.org/10.1016/j.cell.2010.03.033>
- [35] Ingolia NT. Genome-wide translational profiling by ribosome footprinting. *Methods Enzymol* 2010; 470:119-42; PMID:20946809; [http://dx.doi.org/10.1016/S0076-6879\(10\)70006-9](http://dx.doi.org/10.1016/S0076-6879(10)70006-9)
- [36] Marguerat S, Schmidt A, Codlin S, Chen W, Aebersold R, Bahler J. Quantitative analysis of fission yeast transcriptomes and proteomes in proliferating and quiescent cells. *Cell* 2012; 151:671-83; PMID:23101633; <http://dx.doi.org/10.1016/j.cell.2012.09.019>
- [37] Arribere JA, Doudna JA, Gilbert WV. Reconsidering movement of eukaryotic mRNAs between polysomes and P bodies. *Mol Cell* 2011; 44:745-58; PMID:22152478; <http://dx.doi.org/10.1016/j.molcel.2011.09.019>
- [38] Moore PB. How should we think about the ribosome? *Annu Rev Biophys* 2012; 41:1-19; PMID:22577819; <http://dx.doi.org/10.1146/annurev-biophys-050511-102314>
- [39] Tourigny DS, Fernandez IS, Kelley AC, Ramakrishnan V. Elongation factor G bound to the ribosome in an intermediate state of translocation. *Science* 2013; 340:1235490; PMID:23812720; <http://dx.doi.org/10.1126/science.1235490>
- [40] Pulk A, Cate JH. Control of ribosomal subunit rotation by elongation factor G. *Science* 2013; 340:1235970; PMID:23812721; <http://dx.doi.org/10.1126/science.1235970>
- [41] Zhou J, Lancaster L, Donohue JP, Noller HF. Crystal structures of EF-G-ribosome complexes trapped in intermediate states of translocation. *Science* 2013; 340:1236086; PMID:23812722; <http://dx.doi.org/10.1126/science.1236086>
- [42] Nolan RD, Grasmuk H, Drews J. The binding of tritiated elongation factors 1 and 2 to ribosomes from Krebs II mouse ascites tumor cells. *Eur J Biochem* 1975; 50:391-402; PMID:1126342; <http://dx.doi.org/10.1111/j.1432-1033.1975.tb09815.x>
- [43] Mizumoto K, Iwasaki K, Tanaka M, Kaziro Y. Studies on polypeptide elongation factor 2 from pig liver. I. Purification and properties. *J Biochem* 1974; 75:1047-56; PMID:4607115
- [44] Smith KE, Hirsch CA, Henshaw EC. Role of elongation factors and the effect of aurintricarboxylic acid on the synthesis of polyphenylalanine. *J Biol Chem* 1973; 248:122-30; PMID:4692826
- [45] Aspden JL, Eyre-Walker YC, Phillips RJ, Amin U, Mumtaz MA, Brocard M, Couso JP. Extensive translation of small Open Reading Frames revealed by Poly-Ribo-Seq. *Elife* 2014; 3:e03528; PMID:25144939; <http://dx.doi.org/10.7554/eLife.03528>
- [46] Ruiz-Orera J, Messeguer X, Subirana JA, Alba MM. Long non-coding RNAs as a source of new peptides. *Elife* 2014; 3:e03523; PMID:25233276; <http://dx.doi.org/10.7554/eLife.03523>
- [47] Fritsch C, Herrmann A, Nothnagel M, Szafranski K, Huse K, Schumann F, Schreiber S, Platzer M, Krawczak M, Hampe J, et al. Genome-wide search for novel human uORFs and N-terminal protein extensions using ribosomal footprinting. *Genome Res* 2012; 22:2208-18; PMID:22879431; <http://dx.doi.org/10.1101/gr.139568.112>
- [48] Stern-Ginossar N, Weisburd B, Michalski A, Le VT, Hein MY, Huang SX, Ma M, Shen B, Qian SB, Hengel H, et al. Decoding human cytomegalovirus. *Science* 2012; 338:1088-93; PMID:23180859; <http://dx.doi.org/10.1126/science.1227919>

Dynamic m⁶A mRNA methylation directs translational control of heat shock response

Jun Zhou¹, Ji Wan¹, Xiangwei Gao¹, Xingqian Zhang¹, Samie R. Jaffrey² & Shu-Bing Qian¹

The most abundant mRNA post-transcriptional modification is N⁶-methyladenosine (m⁶A), which has broad roles in RNA biology^{1–5}. In mammalian cells, the asymmetric distribution of m⁶A along mRNAs results in relatively less methylation in the 5' untranslated region (5'UTR) compared to other regions^{6,7}. However, whether and how 5'UTR methylation is regulated is poorly understood. Despite the crucial role of the 5'UTR in translation initiation, very little is known about whether m⁶A modification influences mRNA translation. Here we show that in response to heat shock stress, certain adenosines within the 5'UTR of newly transcribed mRNAs are preferentially methylated. We find that the dynamic 5'UTR methylation is a result of stress-induced nuclear localization of YTHDF2, a well-characterized m⁶A 'reader'. Upon heat shock stress, the nuclear YTHDF2 preserves 5'UTR methylation of stress-induced transcripts by limiting the m⁶A 'eraser' FTO from demethylation. Remarkably, the increased 5'UTR methylation in the form of m⁶A promotes cap-independent translation initiation, providing a mechanism for selective mRNA translation under heat shock stress. Using Hsp70 mRNA as an example, we demonstrate that a single m⁶A modification site in the 5'UTR enables translation initiation independent of the 5' end N⁷-methylguanosine cap. The elucidation of the dynamic features of 5'UTR methylation and its critical role in cap-independent translation not only expands the breadth of physiological roles of m⁶A, but also uncovers a previously unappreciated translational control mechanism in heat shock response.

Given the reversible nature of m⁶A mRNA methylation^{8,9}, we sought to assess the potential impact of heat shock stress on m⁶A modification of eukaryotic mRNAs. Using immunofluorescence staining, we first examined the subcellular localization of the entire m⁶A machinery in a mouse embryonic fibroblast (MEF) cell line before and after heat shock stress. It is believed that m⁶A modification occurs primarily at nuclear speckles, whereas its functionality takes place in the cytosol (Fig. 1a). Consistent with this notion, both the m⁶A 'writers' (METTL3, METTL14, WTAP) and the eraser FTO were predominantly present in the nucleus, whereas the majority of the reader YTHDF2 resided in the cytosol (Fig. 1b and Extended Data Fig. 1). In response to heat shock stress, neither the writers nor the eraser changed their nuclear localization (Extended Data Fig. 1). Surprisingly, nearly all of the YTHDF2 molecules were relocated into the nucleus from the cytosol upon heat shock stress (Fig. 1b). The same phenomenon holds true in HeLa cells. Intriguingly, the protein level of YTHDF2 was also markedly increased after heat shock stress in a manner similar to Hsp70 induction (Fig. 1c). In contrast, neither the m⁶A writers nor the eraser showed any differences in protein levels upon stress. Supporting the stress-induced transcriptional upregulation of YTHDF2, real-time PCR revealed a nearly fourfold increase of YTHDF2 abundance after heat shock stress (Fig. 1d). The increased YTHDF2 abundance was not due to altered mRNA degradation since heat shock stress had negligible effects on mRNA stability (Extended Data Fig. 2a). Notably, YTHDF2 exhibited a relatively short half-life ($t_{1/2} < 1$ h) in cells, supporting the importance of stress-induced

transcriptional upregulation. Genes encoding other YTH domain family proteins like YTHDF1 and YTHDF3 also showed upregulation, although to a lesser extent (Extended Data Fig. 2b). Using a mouse fibroblast cell line lacking the heat shock transcription factor 1 (HSF1)¹⁰, we confirmed that YTHDF2 is subject to regulation by HSF1 (Extended Data Fig. 2c). The unexpected stress-inducible feature of YTHDF2 suggests a potential role of m⁶A modification in heat shock response.

Although YTHDF2 primarily serves as the reader of m⁶A, recent proteomic data revealed that YTHDF2 has an extensive physical interaction with the components of m⁶A writers¹¹. Given their co-localization upon heat shock stress, we postulated that the nuclear presence of YTHDF2 could influence the m⁶A modification and alter the landscape of mRNA methylomes. Using an optimized m⁶A-seq procedure^{6,12}, we sequenced the entire methylated RNA species purified from MEF cells with or without heat shock stress. From a total of 15,454 putative methylation sites, we confirmed the m⁶A consensus sequence motif as GGAC (where the underlined A is modified) (Extended Data Fig. 3 and Supplementary Table 1). Consistent with previous reports^{6,7}, the majority of m⁶A sites are enriched in the

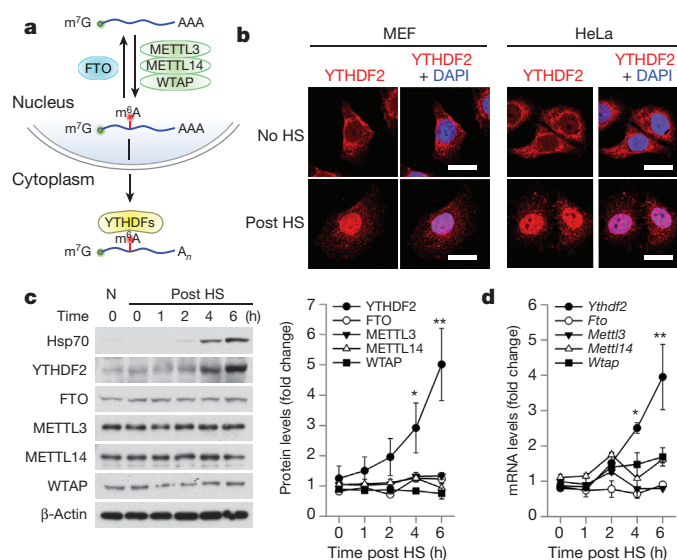


Figure 1 | YTHDF2 changes cellular localization and expression levels in response to heat shock stress. **a**, Schematic of m⁶A modification machinery in mammalian cells. **b**, Subcellular localization of YTHDF2 in MEF and HeLa cells before or 2 h after heat shock (42 °C, 1 h). Bar, 10 μm. Images are representative of at least 50 cells. **c**, Immunoblotting of MEF cells after heat shock stress (42 °C, 1 h). N, no heat shock. The right panel shows the relative protein levels quantified by densitometry and normalized to β-actin. Representative of three biological replicates. **d**, Same samples in **c** were used for RNA extraction and real-time PCR. Relative levels of indicated transcripts are normalized to β-actin. Error bars, mean ± s.e.m.; * $P < 0.05$, ** $P < 0.01$, unpaired two-tailed t -test; $n = 3$ biological replicates (**c** and **d**).

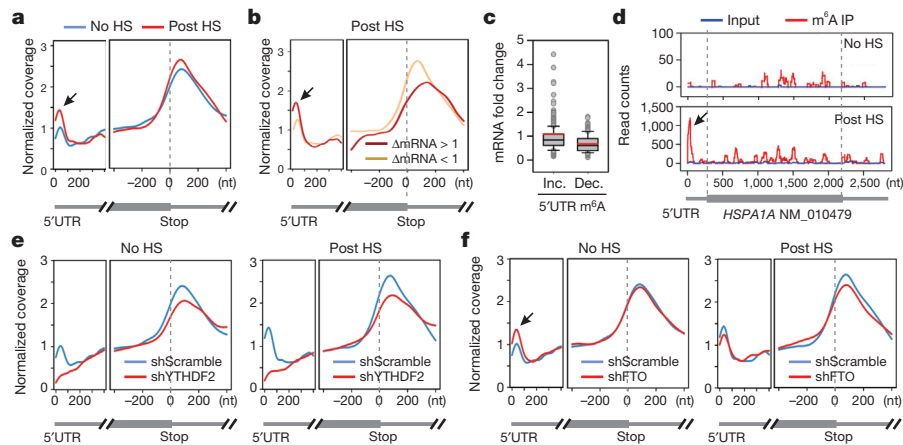


Figure 2 | Altered m⁶A profiles in MEF cells in response to heat shock stress.

a, Metagenes profiles of m⁶A distribution across the transcriptome of cells before or 2 h after heat shock (42 °C, 1 h). Black arrow indicates the m⁶A peak in the 5'UTR region. **b**, Transcripts are stratified by different expression levels after heat shock stress, followed by metagenes profiles of m⁶A distribution. **c**, A box plot depicting fold changes of mRNA levels after heat shock for transcripts showing increased or decreased m⁶A modification in the 5'UTR.

vicinity of the stop codon and in the 3'UTR (Fig. 2a). Unexpectedly, heat shock stress led to an elevated m⁶A peak in the 5'UTR, but not other regions. Reasoning that only a handful of genes undergo upregulation as a result of heat shock response^{13,14}, we compared the levels of m⁶A modification between stress-inducible and non-inducible transcripts defined by RNA-seq. It is clear that the upregulated transcripts showed greater m⁶A modification in the 5'UTR than the transcripts downregulated upon stress (Fig. 2b). We next stratified transcripts based on differential changes of m⁶A modification in the 5'UTR. While transcripts with elevated 5'UTR methylation are mostly upregulated in response to stress, transcripts exhibiting decreased 5'UTR methylation are largely downregulated (Fig. 2c, $P < 0.001$, Mann–Whitney Test). One particular example of stress-induced transcripts is the Hsp70 gene *HSPA1A*, which not only showed a 90-fold increase of mRNA levels after heat shock, but also displayed a prominent m⁶A peak in the 5'UTR (Fig. 2d). By contrast, the constitutively expressed Hsc70 gene *HSPA8* showed only minor increase in both the mRNA level and the m⁶A modification in response to heat shock stress (Extended Data Fig. 4). These results suggest that the increased 5'UTR methylation selectively occurs on the stress-inducible mRNAs.

To examine whether the elevated 5'UTR methylation upon heat shock stress is a result of nuclear localization of YTHDF2, we silenced YTHDF2 in MEF cells using lentiviruses expressing short hairpin RNAs. Remarkably, MEF cells lacking YTHDF2 demonstrated a substantial loss of m⁶A modification in the 5'UTR (Fig. 2e). Upon heat shock stress, these cells no longer showed the elevated 5'UTR methylation as seen in control cells. The abolished 5'UTR methylation in the absence of YTHDF2 was clearly exemplified in *HSPA1A* that exhibited only background m⁶A modification in the 5'UTR (Extended Data Fig. 5). This result indicates a novel function of YTHDF2 in heat shock response by promoting 5'UTR methylation on mRNAs transcribed during stress.

YTHDF2 is not a methyltransferase *per se*, and does not bind to mRNAs without prior m⁶A modification³⁷. How does the nuclear presence of YTHDF2 promote selective methylation in the 5'UTR? One possibility is that YTHDF2 protects the pre-existing m⁶A from FTO-mediated demethylation. Upon heat shock stress, the nuclear localization of YTHDF2 probably limits the accessibility of FTO to newly minted m⁶A sites, thereby tilting the equilibrium towards methylation. Indeed, an *in vitro* m⁶A binding and demethylation assay confirmed direct competition between FTO and YTHDF2 (Extended Data Fig. 6). To investigate whether FTO preferentially removes m⁶A

Box plot centre line (black), mean; whiskers, 5th and 95th percentiles; red line, median. **d**, An example of stress-induced transcript *HSPA1A* harbouring m⁶A peaks. IP, immunoprecipitation. **e**, Metagenes profiles of m⁶A distribution across the transcriptome of cells with or without YTHDF2 knockdown, before or after heat shock stress. **f**, Metagenes profiles of m⁶A distribution across the transcriptome of cells with or without FTO knockdown, before or after heat shock stress.

modification from the 5'UTR, we knocked down FTO from MEF cells and examined the m⁶A distribution across the entire transcriptome. Notably, only the 5'UTR region showed an increase of m⁶A density in cells lacking FTO (Fig. 2f). Additionally, the 5'UTR methylation showed no further increase upon heat shock stress in the absence of FTO.

The 5'UTR is crucial in mediating translation initiation of eukaryotic mRNAs^{15,16}. Under stress conditions, the cap-dependent translation is generally suppressed. However, subsets of transcripts are selectively translated via a poorly understood cap-independent mechanism^{17–19}. To investigate whether differential methylation of 5'UTR influences the translational status of these mRNAs, we conducted ribosome profiling of MEF cells with or without heat shock stress. Among the genes undergoing stress-induced transcriptional upregulation, many not only showed elevated m⁶A modification in the 5'UTR, but also demonstrated increased ribosome occupancy in the coding region (Fig. 3a). Several prominent examples are genes encoding heat shock proteins, in particular Hsp70 (Supplementary Table 2). Therefore, the coordinated upregulation of transcription and 5'UTR methylation is coupled with robust translation in response to heat shock stress.

To validate the causal relationship between stress-induced 5'UTR methylation and selective translation, we examined Hsp70 synthesis in cells with differential m⁶A modification. Knocking down YTHDF2 leads to depleted 5'UTR methylation, as revealed by m⁶A-seq (Fig. 2e). Indeed, direct m⁶A blotting of *HSPA1A* purified from heat-shock-stressed MEFs confirmed the marked reduction of methylation in cells lacking YTHDF2 (Fig. 3b). Remarkably, the heat-shock-induced Hsp70 synthesis was substantially reduced in the absence of YTHDF2 (Fig. 3c). The comparable Hsp70 mRNA levels in cells with or without YTHDF2 knockdown indicate that the reduced Hsp70 synthesis is a result of translational deficiency (Extended Data Fig. 7). Further supporting this notion, the Hsp70 transcript, but not GAPDH, showed much less enrichment in the polysomes of MEF cells lacking YTHDF2 (Fig. 3d).

Reasoning that YTHDF2 competes with FTO in preserving 5'UTR m⁶A modification, we speculated that FTO knockdown would increase the 5'UTR methylation as well as the translation efficiency of Hsp70 mRNA. This was indeed the case. Direct m⁶A blotting of *HSPA1A* purified from stressed MEFs lacking FTO revealed a clear increase of methylation when compared to the scramble control (Extended Data Fig. 8). Importantly, FTO knockdown potentiated

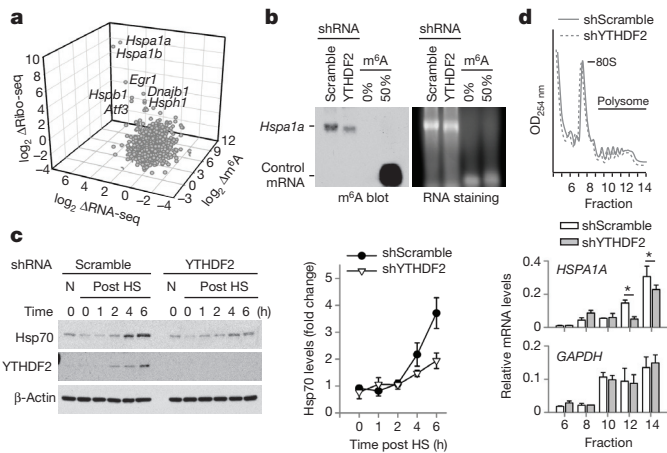


Figure 3 | m^6A modification promotes selective translation under heat shock stress. **a**, A 3D plot depicting fold changes (\log_2) of mRNA abundance, coding sequence ribosome occupancy (Ribo-seq), and 5'UTR m^6A levels in MEF cells after heat shock stress. **b**, m^6A blotting of *HSPA1A* purified from MEFs with or without YTHDF2 knockdown. Messenger RNAs synthesized by *in vitro* transcription in the absence or presence of m^6A were used as control. Images are representative of two biological replicates. **c**, Immunoblotting of MEF cells with or without YTHDF2 knockdown after heat shock stress (42 °C, 1 h). N, no heat shock. The right panel shows the relative protein levels quantified by densitometry and normalized to β -actin. Blots are representative of three biological replicates. **d**, MEF cells with or without YTHDF2 knockdown were subject to heat shock stress followed by sucrose gradient sedimentation. Specific mRNA levels in polysome fractions were measured by quantitative PCR. The values are first normalized to the spike in control then to the total. Error bars, mean \pm s.e.m.; * P < 0.05, unpaired two-tailed t -test; n = 3 biological replicates (c and d).

the synthesis of Hsp70 after heat shock stress. Collectively, these results established the functional connection between dynamic 5'UTR methylation and selective mRNA translation during stress.

It is commonly believed that the 5'UTR of Hsp70 mRNA recruits the translational machinery via an internal ribosome entry site (IRES)^{20–23}. However, conflicting results exist and the exact cap-independent translation-promoting determinants remain elusive^{23,24}. Given the fact that the normal 5' end cap structure is a methylated purine (N^7 -methylguanosine, m^7G), we hypothesize that the stress-induced m^6A in the 5'UTR enables selective translation by acting as a functional cap substitute. To test this hypothesis, we performed a firefly luciferase (Fluc) reporter assay in MEF cells by transfecting mRNAs synthesized in the absence or presence of m^6A (Fig. 4a). For the messenger without 5'UTR, random incorporation of m^6A slightly reduced the Fluc activity after mRNA transfection. In the presence of 5'UTR from Hsp70, but not tubulin, the incorporation of m^6A markedly increased the Fluc activity in transfected MEF cells. Notably, m^6A incorporation does not affect the stability of the synthesized mRNAs in transfected cells (Extended Data Fig. 9a). We next replaced the 5' end m^7G cap with a non-functional cap analogue ApppG. As expected, the resultant mRNA did not support translation in the absence of 5'UTR or in the presence of tubulin 5'UTR (Fig. 4a and Extended Data Fig. 9b). Only when the Hsp70 5'UTR was present, was the translating-promoting feature clearly manifested after m^6A incorporation, in particular under stress conditions (Fig. 4a). This effect is specific to m^6A modification but not m^6Am because ribose methylation in the form of 2'-O-MeA suppressed translation of the Fluc reporter bearing Hsp70 5'UTR (Fig. 4a). Therefore, methylation of Hsp70 5'UTR in the form of m^6A promotes cap-independent translation.

To further demonstrate the 5'UTR specificity in m^6A -facilitated cap-independent translation, we examined 5'UTRs from a constitutively expressed chaperone Hsc70 (*HSPA8*) and another stress-inducible chaperone Hsp105 (*HSPH1*) (Fig. 3a). Only the 5'UTR of

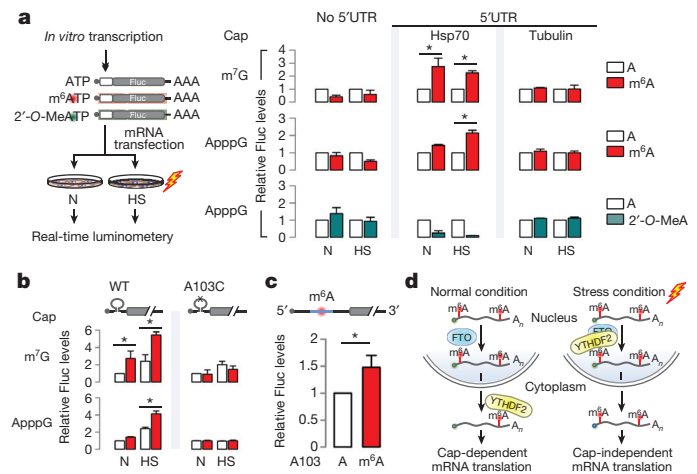


Figure 4 | Selective 5'UTR m^6A modification mediates cap-independent translation. **a**, MEF cells transfected with Fluc mRNA reporters were subject to heat shock treatment and the Fluc activity was measured by real-time luminometry. Fluc activities were quantified and normalized to the sample containing normal adenosine nucleotides. Red, m^6A ; green, 2'-O-MeA. **b**, Constructs expressing Fluc reporter with Hsp70 5'UTR or the one with A103C mutation are depicted on the top. Fluc activities in transfected MEF cells were quantified and normalized to the control containing normal A without stress. **c**, Fluc mRNAs bearing Hsp70 5'UTR with a single m^6A site were constructed using sequential splint ligation. After *in vitro* translation in rabbit reticulocyte lysates, Fluc activities were quantified and normalized to the control lacking m^6A . Error bars, mean \pm s.e.m.; * P < 0.05, unpaired two-tailed t -test; n = 3 biological replicates (a, b and c). **d**, A proposed model for dynamic m^6A 5'UTR methylation in response to stress and its role in cap-independent translation. Under the normal growth condition, nuclear FTO demethylates the 5'UTR m^6A from nascent transcripts and the matured transcripts are translated via a cap-dependent mechanism. Under stress conditions, nuclear localization of YTHDF2 protects the 5'UTR of stress-induced transcripts from demethylation. With enhanced 5'UTR methylation, these transcripts are selectively translated via a cap-independent mechanism.

Hsp105 enhanced translation of the non-capped message after m^6A incorporation (Extended Data Fig. 9c). This result is consistent with the selective 5'UTR methylation of stress-inducible transcripts upon heat shock stress.

The 5'UTR contains multiple As, although not all of them are methylated. On the basis of the predicted m^6A sequence motif, the A residue at the 103 position of Hsp70 mRNA is likely to be methylated. Using a single-nucleotide m^6A detection method²⁵, we confirmed the methylation event at this position upon heat shock stress (Extended Data Fig. 10a). To demonstrate the significance of methylation at this single site, we introduced an A103C mutation into the Hsp70 5'UTR. Remarkably, m^6A incorporation no longer promoted translation of the Fluc reporter in transfected cells (Fig. 4b). To directly demonstrate the importance of this single m^6A site without changing the nucleotide, we employed a sequential RNA splint ligation strategy to construct a Fluc reporter bearing Hsp70 5'UTR with or without A103 methylation (Fig. 4c)^{26,27}. Using an *in vitro* translation system, the Fluc reporter containing the single m^6A at the 103 position showed about 50% increase in translation efficiency in comparison to the one with normal A (Fig. 4c). Notably, both messages showed comparable turnover during the entire course of *in vitro* translation (Extended Data Fig. 10c). Collectively, these results firmly established a crucial role of 5'UTR m^6A modification in non-canonical translation initiation.

Much of our current understanding of cap-independent translation is limited to the IRES mechanism^{28,29}. However, beyond a few examples, many cellular genes capable of cap-independent translation do not seem to contain any IRES elements. The results presented here demonstrate a surprising role of m^6A in mediating mRNA translation initiation independent of the normal m^7G cap. How exactly the

methylated adenosine recruits the translation machinery merits further investigation. m⁶A modification has been shown to alter RNA secondary structures⁴. It is possible that distinct translation initiation factors are recruited to the methylated 5'UTR, thereby facilitating cap-independent translation.

In contrast to the wide belief that m⁶A modification is static on mRNAs, we found that 5'UTR methylation in the form of m⁶A is dynamic. Methylation often serves as a mark to distinguish self and foreign DNAs or parental and daughter DNA strands³⁰. The stress-inducible mRNA 5'UTR methylation permits ribosomes to distinguish nascent transcripts from pre-existing messages, thereby achieving selective mRNA translation (Fig. 4d). The unexpected stress-inducible feature of YTHDF2 offers an elegant mechanism for temporal control of m⁶A modification on subsets of mRNAs. The mechanistic connection between 5'UTR methylation and cap-independent translation solves the central puzzle how selective translation is achieved when global translation is suppressed in responding to stress.

Online Content Methods, along with any additional Extended Data display items and Source Data, are available in the online version of the paper; references unique to these sections appear only in the online paper.

Received 23 February; accepted 30 July 2015.

Published online 12 October 2015.

- Meyer, K. D. & Jaffrey, S. R. The dynamic epitranscriptome: N⁶-methyladenosine and gene expression control. *Nature Rev. Mol. Cell Biol.* **15**, 313–326 (2014).
- Fu, Y., Dominissini, D., Rechavi, G. & He, C. Gene expression regulation mediated through reversible m⁶A RNA methylation. *Nature Rev. Genet.* **15**, 293–306 (2014).
- Wang, X. *et al.* N⁶-methyladenosine-dependent regulation of messenger RNA stability. *Nature* **505**, 117–120 (2014).
- Liu, N. *et al.* N⁶-methyladenosine-dependent RNA structural switches regulate RNA-protein interactions. *Nature* **518**, 560–564 (2015).
- Wang, X. *et al.* N⁶-methyladenosine modulates messenger RNA translation efficiency. *Cell* **161**, 1388–1399 (2015).
- Meyer, K. D. *et al.* Comprehensive analysis of mRNA methylation reveals enrichment in 3' UTRs and near stop codons. *Cell* **149**, 1635–1646 (2012).
- Dominissini, D. *et al.* Topology of the human and mouse m⁶A RNA methylomes revealed by m⁶A-seq. *Nature* **485**, 201–206 (2012).
- Jia, G. *et al.* N⁶-methyladenosine in nuclear RNA is a major substrate of the obesity-associated FTO. *Nature Chem. Biol.* **7**, 885–887 (2011).
- Zheng, G. *et al.* ALKBH5 is a mammalian RNA demethylase that impacts RNA metabolism and mouse fertility. *Mol. Cell* **49**, 18–29 (2013).
- Qian, S. B., McDonough, H., Boellmann, F., Cyr, D. M. & Patterson, C. CHIP-mediated stress recovery by sequential ubiquitination of substrates and Hsp70. *Nature* **440**, 551–555 (2006).
- Schwartz, S. *et al.* Perturbation of m⁶A writers reveals two distinct classes of mRNA methylation at internal and 5' sites. *Cell Rep.* **8**, 284–296 (2014).
- Schwartz, S. *et al.* High-resolution mapping reveals a conserved, widespread, dynamic mRNA methylation program in yeast meiosis. *Cell* **155**, 1409–1421 (2013).
- Ankar, J. & Sistonen, L. Regulation of HSF1 function in the heat stress response: implications in aging and disease. *Annu. Rev. Biochem.* **80**, 1089–1115 (2011).
- Mendillo, M. L. *et al.* HSF1 drives a transcriptional program distinct from heat shock to support highly malignant human cancers. *Cell* **150**, 549–562 (2012).
- Jackson, R. J., Hellen, C. U. & Pestova, T. V. The mechanism of eukaryotic translation initiation and principles of its regulation. *Nature Rev. Mol. Cell Biol.* **11**, 113–127 (2010).
- Hinnebusch, A. G. The scanning mechanism of eukaryotic translation initiation. *Annu. Rev. Biochem.* **83**, 779–812 (2014).
- Spriggs, K. A., Bushell, M. & Willis, A. E. Translational regulation of gene expression during conditions of cell stress. *Mol. Cell* **40**, 228–237 (2010).
- Panniers, R. Translational control during heat shock. *Biochimie* **76**, 737–747 (1994).
- Richter, K., Haslbeck, M. & Buchner, J. The heat shock response: life on the verge of death. *Mol. Cell* **40**, 253–266 (2010).
- McGarry, T. J. & Lindquist, S. The preferential translation of *Drosophila* hsp70 mRNA requires sequences in the untranslated leader. *Cell* **42**, 903–911 (1985).
- Klemenz, R., Hultmark, D. & Gehring, W. J. Selective translation of heat shock mRNA in *Drosophila melanogaster* depends on sequence information in the leader. *EMBO J.* **4**, 2053–2060 (1985).
- Rubtsova, M. P. *et al.* Distinctive properties of the 5'-untranslated region of human hsp70 mRNA. *J. Biol. Chem.* **278**, 22350–22356 (2003).
- Sun, J., Conn, C. S., Han, Y., Yeung, V. & Qian, S. B. PI3K–mTORC1 attenuates stress response by inhibiting cap-independent Hsp70 translation. *J. Biol. Chem.* **286**, 6791–6800 (2011).
- Zhang, X. *et al.* Translational control of the cytosolic stress response by mitochondrial ribosomal protein L18. *Nature Struct. Mol. Biol.* **22**, 404–410 (2015).
- Harcourt, E. M., Ehrenschröder, T., Batista, P. J., Chang, H. Y. & Kool, E. T. Identification of a selective polymerase enables detection of N⁶-methyladenosine in RNA. *J. Am. Chem. Soc.* **135**, 19079–19082 (2013).
- Kershaw, C. J. & O'Keefe, R. T. Splint ligation of RNA with T4 DNA ligase. *Methods Mol. Biol.* **941**, 257–269 (2012).
- Stark, M. R., Pleiss, J. A., Deras, M., Scaringe, S. A. & Rader, S. D. An RNA ligase-mediated method for the efficient creation of large, synthetic RNAs. *RNA* **12**, 2014–2019 (2006).
- Pelletier, J. & Sonenberg, N. Internal initiation of translation of eukaryotic mRNA directed by a sequence derived from poliovirus RNA. *Nature* **334**, 320–325 (1988).
- Hellen, C. U. & Sarnow, P. Internal ribosome entry sites in eukaryotic mRNA molecules. *Genes Dev.* **15**, 1593–1612 (2001).
- Kunkel, T. A. & Erie, D. A. DNA mismatch repair. *Annu. Rev. Biochem.* **74**, 681–710 (2005).

Supplementary Information is available in the online version of the paper.

Acknowledgements We would like to thank Qian laboratory members for helpful discussions and Cornell University Life Sciences Core Laboratory Center for performing deep sequencing. This work was supported by grants from the US National Institutes of Health DP2 OD006449 and R01AG042400 (to S.-B.Q.) and NIDA DA037150 (to S.R.J.) and the US Department of Defense (W81XWH-14-1-0068) (to S.-B.Q.).

Author Contributions J.Z. and S.-B.Q. conceived the project. J.Z. performed most experiments. J.W. analysed the sequencing data. X.G. performed Ribo-seq. X.Z. assisted heat shock assays. S.R.J. helped with original FTO ideas. S.-B.Q. wrote the manuscript. All authors discussed the results and edited the manuscript.

Author Information Sequencing data have been deposited at NCBI Sequence Read Archive under accession number SRA280261. Reprints and permissions information is available at www.nature.com/reprints. The authors declare no competing financial interests. Readers are welcome to comment on the online version of the paper. Correspondence and requests for materials should be addressed to S.-B.Q. (sq38@cornell.edu).

METHODS

No statistical methods were used to predetermine sample size. The experiments were not randomized and the investigators were not blinded to allocation during experiments and outcome assessment.

Cell lines and reagents. HeLa (cervical cancer) was originally purchased from ATCC and MEF cells were a gift from D. J. Kwiatkowski (Harvard Medical School). Cells were not authenticated recently but tested negative for mycoplasma contamination. Both cells were maintained in Dulbecco's Modified Eagle's Medium (DMEM) with 10% fetal bovine serum (FBS). Antibodies used in the experiments are listed below: anti-YTHDF2 (Proteintech 24744-1-AP, 1:1,000 WB, 1:600 IF); anti-Hsp70 (Stressgen SPA-810, 1:1,000 WB); anti-FTO (Phosphosolutions 597-Fto, 1:1,000 WB, 1:600 IF); anti-METTL3 (Abnova H00056339-B01P, 1:1,000 WB, 1:600 IF); anti-METTL14 (sigma HPA038002, 1:1,000 WB, 1:600 IF); anti-WTAP (Santa Cruz sc-374280, 1:1,000 WB, 1:600 IF); anti-m⁶A (Millipore ABE572, 1:1,000 m⁶A immunoblotting); Alexa Fluor 546 donkey anti-mouse secondary antibody (Invitrogen A10036, 1:600 IF); Alexa Fluor 546 donkey anti-rabbit secondary antibody (Invitrogen A10040, 1:600 IF).

Construction of 5' UTR reporters. The Fluc reporter with Hsp70 5' UTR has been reported previously²³. For Fluc reporters bearing other 5' UTRs, the following primers were used for 5' UTR cloning: Hsc70 (*HSPA8*) forward, 5'-CCCAA GCTTGGTCTCATTGAACGCGG-3'; reverse, 5'-CGGGATCCCCTTAGACA TGGTTGCTT-3'; Tubulin (*TUBG2*) forward, 5'-GGCAAGCTTTGCGCCTGT GCTGAATTCCAGCTGC-3'; reverse, 5'-GGCGGATCCGCATCGCCGATCA CAGCTAG-3'; Hsp105 (*HSPH1*) forward, 5'-CCCAAGCTTGTAAATGCTG CAGATTTC-3'; reverse, 5'-CGGGATCCCCACCGACATGGTGGCCCG-3'.

Lentiviral shRNAs. All shRNA targeting sequences were cloned into DECIPHER pRSI9-U6-(sh)-UbiC-TagRFP-2A-Puro (Collecta). shRNA targeting sequences listed below were based on RNAi consortium at Broad Institute (<http://www.broad.mit.edu/rnai/trc>). YTHDF2 (mouse): 5'-GCTCCAGGCATGAATA CTATA-3'; FTO (mouse): 5'-GCTGAGGCAGTTCTGGTTTCA-3'; Scramble control sequence: 5'-AACAGTCGCGTTTGGCACTGG-3'. Lentiviral particles were packaged using Lenti-X 293T cells (Clontech). Virus-containing supernatants were collected at 48 h after transfection and filtered to eliminate cells. MEF cells were infected by the lentivirus for 48 h before selection by 1 µg ml⁻¹ puromycin.

Recombinant protein expression. YTHDF2 and FTO were cloned into vector pGEX-6P-1 using the following primers: YTHDF2 forward, 5'-ATGAATTCCC ATCGGCCAGCAGCCTCTTG-3'; reverse, 5'-CCGCTCGAGTTCTATTCCC ACGACCTGA-3'; FTO forward, 5'-ATGAATTCAGCATGAAGCGCGTCC AGACC-3'; reverse, 5'-CCGCTCGAGCCTCTAGGATCTTGC-3'.

The resulting clones were transfected into the *Escherichia coli* strain BL21 and expression was induced at 22 °C with 1 mM IPTG for 16–18 h. The pellet collected from 1 l of bacteria culture was then lysed in 15 ml PBS (50 mM NaH₂PO₄, 150 mM NaCl, pH 7.2, 1 mM PMSF, 1 mM DTT, 1 mM EDTA, 0.1% (v/v) Triton X-100) and sonicated for 10 min. After removing cell debris by centrifugation at 12,000 r.p.m. for 30 min, the protein extract was mixed with 2 ml equilibrated Pierce glutathione agarose and mixed on an end-over-end rotator for 2 h at 4 °C. The resin was washed three times with ten resin-bed volumes of equilibration/wash buffer (50 mM Tris, 150 mM NaCl, pH 8.0). YTHDF2 and FTO protein was cleaved from the glutathione agarose using PreScission Protease (Genscript) in cleavage buffer (50 mM Tris-HCl, pH 7.0, 150 mM NaCl, 1 mM EDTA, 1 mM DTT) at 4 °C overnight.

Immunoblotting. Cells were lysed on ice in TBS buffer (50 mM Tris, pH 7.5, 150 mM NaCl, 1 mM EDTA) containing protease inhibitor cocktail tablet, 1% Triton X-100, and 2 U ml⁻¹ DNase. After incubating on ice for 30 min, the lysates were heated for 10 min in SDS/PAGE sample buffer (50 mM Tris (pH 6.8), 100 mM dithiothreitol, 2% SDS, 0.1% bromophenol blue, 10% glycerol). Proteins were separated on SDS-PAGE and transferred to Immobilon-P membranes (Millipore). Membranes were blocked for 1 h in TBS containing 5% non-fat milk and 0.1% Tween-20, followed by incubation with primary antibodies overnight at 4 °C. After incubation with horseradish-peroxidase-coupled secondary antibodies at room temperature for 1 h, immunoblots were visualized using enhanced chemiluminescence (ECL^{Plus}, GE Healthcare).

Immunofluorescence staining. Cells grown on glass coverslips were fixed in 4% paraformaldehyde for 10 min at 4 °C. After permeabilization in 0.2% Triton X-100 for 5 min at room temperature, the cover slips were blocked with 1% BSA for 1 h. Cells were stained with indicated primary antibody overnight at 4 °C, followed by incubation with Alexa Fluor 546 donkey anti-mouse secondary antibody or Alexa Fluor 546 donkey anti-rabbit secondary antibody for 1 h at room temperature. The nuclei were counter-stained with DAPI (1:1,000 dilution) for 10 min. Cover slips were mounted onto slides and visualized using a Zeiss LSM710 confocal microscope.

mRNA stability measurement. Cells were treated with actinomycin D (5 µg ml⁻¹) for 4 h, 2 h and 0 h before trypsinization and collection. RNA spike-in control was added proportional to the total cell numbers and total RNA was isolated by TRIzol kit (Life Technologies). After reverse transcription, the mRNA levels of transcripts of interest were detected by real-time quantitative PCR.

Real-time quantitative PCR. Total RNA was isolated by TRIzol reagent (Invitrogen) and reverse transcription was performed using High Capacity cDNA Reverse Transcription Kit (Invitrogen). Real-time PCR analysis was conducted using Power SYBR Green PCR Master Mix (Applied Biosystems) and carried on a LightCycler 480 Real-Time PCR System (Roche Applied Science). Primers for amplifying each target were: YTHDF2 forward, 5'-CAGTTTGCCCT CCAGCTACTATT-3'; reverse, 5'-GCAATGCCATTCTTGGTCTTC-3'; FTO forward, 5'-TCAGCAGTGGCAGCTGAAAT-3'; reverse, 5'-CTTGGATCCTC ACCACGTCC-3'; Hsp70 forward, 5'-TGGTGCAGTCCGACATGAAG-3'; reverse, 5'-GCTGAGAGTCGTGAAGTAGGC-3'; METTL3 forward, 5'-ATC CAGGCCATAAGAAACAG-3'; reverse, 5'-CTATCACTACGGAAGGTTG GG-3'; METTL14 forward, 5'-CAGGCAGAGCATGGGATATT-3'; reverse, 5'-TCCGACCTGGAGACATACAT-3'; ALKBH5 forward, 5'-AGTTCAGGTTT CAGCCATC-3'; reverse, 5'-GGCGTTCTTAATGTCCTGAG-3'; WTAP forward, 5'-CTGGCAGAGGAGGTAGTAGTTA-3'; reverse, 5'-ACTGGAGTCTG TGTCATTTGAG-3'; β-actin forward, 5'-TTGCTGACAGGATGCAGAAAG-3'; reverse, 5'-ACTCCTGCTTGCTGATCCACAT-3'; GAPDH forward, 5'-CAAG GAGTAAGAAACCCCTGGAC-3'; reverse, 5'-GGATGGAAATTTGTGAGGGAG AT-3'; Fluc forward, 5'-ATCCGGAAGCGACCAACGCC-3'; reverse, 5'-GTCC GGAAGACCTGCCACGC-3'.

In vitro transcription. Plasmids containing the corresponding 5' UTR sequences of mouse *HSPA1A* and full-length firefly luciferase were used as templates. Transcripts with normal m⁷G cap were generated using the mMessage mMachine T7 Ultra kit (Ambion) and transcripts with non-functional cap analogue GpppA were synthesized using MEGascript T7 Transcription Kit (Ambion). To obtain mRNAs with the adenosine replaced with m⁶A, *in vitro* transcription was conducted in a reaction in which 5% of the adenosine was replaced with N⁶-methyladenosine. All mRNA products were purified using the MEGAclear kit (Ambion) according to the manufacturer's instructions.

In vitro translation. *In vitro* translation was performed using the Rabbit Reticulocyte Lysate System (Promega) according to the manufacturer's instructions. Luciferase activity was measured using a luciferase reporter assay system (Promega) on a Synergy HT Multi-detection Microplate Reader (BioTek Instruments).

Real-time luciferase assay. Cells grown in 35-mm dishes were transfected with *in-vitro*-synthesized mRNA containing the luciferase gene. Luciferase substrate D-luciferin (1 mM, Regis Tech) was added into the culture medium immediately after transfection. Luciferase activity was monitored and recorded using Kronos Dio Lumometer (Atto).

Site-specific m⁶A detection. For site-specific m⁶A detection, DNA primers were first 5' labelled with ³²P using T4 polynucleotide kinase (Invitrogen) and purified by ethanol precipitation. The primer 5'-AGGGATGCTCTGGGGAAGGCTGG-3' was used to detect potential m⁶A site and the primer 5'-CGCCGCTCG CTCTGCTTCTCTTGTCTTCGCT-3' was used to detect the non-methylated site. Synthesized mRNA 5'-CGATCCTCGGCCAGG(m⁶A)CCAGCCTTCCCC AG-3' and 5'-CGATCCTCGGCCAGGACCAGCCTTCCCCAG-3' served as positive and negative control templates, respectively. To set up the reaction, a 2 × annealing solution was prepared in a total volume of 8 µl with 1 × Tth buffer (Promega) or AMV buffer (Invitrogen), 1 µl of each radiolabelled primer and 10 µg mRNA from MEF cells that had been heat shock treated. The mixture was heated at 95 °C for 10 min and cooled slowly to room temperature. 3 µl of annealing solution were combined with 2 µl of enzyme and heated at 37 °C (AMV Reverse Transcriptase) or 55 °C (Tth DNA Polymerase) for 2 min. After adding the dTTP solution (final dTTP concentration: 100 µM), the reactions were heated for 5 min at 37 °C (AMV) or 10 min at 55 °C (Tth). Reaction products were resolved on a 20% denaturing polyacrylamide gel and exposed overnight.

RNA splint ligation. The ligation method was optimized from previous reports^{26,27,31}. The RNA oligonucleotide covering the 82–117 nt region of *HSPA1A* was synthesized by Thermo Scientific, whereas RNA fragments corresponding to other regions were generated by *in vitro* transcription. For sequential splint ligation, two DNA bridging oligonucleotides were designed: DNA Bridge 1, 5'-GGTCTCTGGCCGAGGATCGGGAACGCCGCTCGCTC-3'; DNA Bridge 2, 5'-CTCCGCGCAGGGATGCTCTGGGGAAGGCTGGTCTC-3'.

For 3' RNA oligonucleotide (donor) phosphorylation, 1 µl of 20 µM donor oligonucleotide was mixed with 1 µl of 10 × PNK buffer, 6 µl of ATP (10 mM), 0.5 µl of RNasin (20 units) and 1 µl of T4 PNK (5 units). The reaction mixture was incubated at 37 °C for 30 min followed by inactivation of T4 PNK at 65 °C for 20 min. Next, the DNA bridge oligonucleotide was hybridized with the 3' RNA

oligonucleotide and the 5' RNA oligonucleotide (acceptor) at a 1:1.5:2 ratio (5' RNA:bridge:3' RNA). Oligonucleotides were annealed (95 °C for 1 min followed by 65 °C for 2 min and 37 °C for 10 min) in the presence of 1 × T4 DNA dilution buffer. To ligate the 5' and the 3' RNA together, T4 DNA ligase and the T4 DNA ligation buffer were added and the reaction mixture was incubated at 37 °C for 1 h. The ligation was stopped by adding 1 µl of 0.5 M EDTA followed by phenol-chloroform extraction and ethanol precipitation. Ligation products were analysed by 10% TBE-Urea gels or formaldehyde gels. The expected RNA ligation products in TBE-Urea gels were eluted in RNA gel elution buffer (300 mM NaOAc pH 5.5, 1 mM EDTA and 0.1 U µl⁻¹ SUPERase_In) followed by ethanol precipitation. The final products in formaldehyde gels were isolated by Zymoclean Gel RNA Recovery Kit (Zymo Research).

Hsp70 mRNA pull-down and m⁶A immunoblotting. To isolate endogenous Hsp70 mRNA, 400 pmol of biotin-labelled probe (5'-TTCATAACATATCTCTGTCTCTT-3') was incubated with 2 mg M-280 Streptavidin Dynabeads (Life Technologies) in 1 ml 1 × B & W buffer (5 mM Tris-HCl pH 7.5, 0.5 mM EDTA and 1 M NaCl) at 4 °C for 1 h. 2 mg total RNA was denatured at 75 °C for 2 min and added to the pre-coated Dynabeads for an additional incubation of 2 h at 4 °C. Captured RNA was eluted by heating beads for 2 min at 90 °C in 10 mM EDTA with 95% formamide followed by TRIzol LS isolation. Isolated RNA was quantified using NanoDrop ND-1000 UV-Vis Spectrophotometer and equal amounts of RNAs were mixed with 2 × RNA Loading Dye (Thermo Scientific) and denatured for 3 min at 70 °C. *In-vitro*-transcribed mRNA containing 50% N⁶-methyladenosine or 100% adenosine was used as positive and negative control, respectively. Samples were separated on a formaldehyde denaturing agarose gel and transferred to a positively charged nylon membrane by siphonage in transfer buffer (10 mM NaOH, 3 M NaCl) overnight at room temperature. After transfer, the membrane was washed for 5 min in 2 × SSC buffer and RNA was UV cross-linked to the membrane. Membrane was blocked for 1 h in PBST containing 5% non-fat milk and 0.1% Tween-20, followed by incubation with anti-m⁶A antibody (1:1,000 dilution) for overnight at 4 °C. After extensive washing with 0.1% PBST three times, the membrane was incubated with HRP-conjugated anti-rabbit IgG (1:5,000 dilution) for 1 h. Membrane was visualized by using enhanced chemiluminescence (ECLPlus, GE Healthcare).

YTHDF2 and FTO *in vitro* pull down. Synthesize mRNA (100 pmol) with a single m⁶A at A103 was label by biotin using the Pierce RNA 3' End Desthiobiotinylation Kit. Binding of the labelled RNA to streptavidin magnetic beads was performed in RNA capture buffer (20 mM Tris, pH 7.5, 1 M NaCl, 1 mM EDTA) for 30 min at room temperature with rotation. The RNA-protein binding reaction was conducted in protein-RNA binding buffer (20 mM Tris (pH 7.5), 50 mM NaCl, 2 mM MgCl₂, 0.1% Tween-20 Detergent) at 4 °C for 60 min with rotation. After washing three times with the wash buffer (20 mM Tris pH 7.5, 10 mM NaCl, 0.1% Tween-20 Detergent), protein was eluted by Biotin Elution Buffer (Pierce) and detected by western blot.

YTHDF2 and FTO *in vitro* competition assay. The YTHDF2 and FTO *in vitro* competition assay was performed in 100 µl of reaction mixture containing 5 µM RNA incorporated with 50% m⁶A, 283 µM of (NH₄)₂Fe(SO₄)₂·6H₂O, 300 µM of α-KG, 2 mM of L-ascorbic acid, 50 µg ml⁻¹ of BSA, and 50 mM of HEPES buffer (pH 7.0). The reaction was incubated for 3 h at room temperature, and quenched by adding 5 mM EDTA followed by heating for 5 min at 95 °C. RNA was isolated by TRIzol LS and quantified using NanoDrop ND-1000 UV-Vis Spectrophotometer. Equal amounts of RNA were used for dot blotting and methylene blue staining was used to show the amount of RNA on hybridization membranes.

Polysome profiling analysis. Sucrose solutions were prepared in polysome buffer (10 mM HEPES, pH 7.4, 100 mM KCl, 5 mM MgCl₂, 100 µg ml⁻¹ cycloheximide and 2% Triton X-100). A 15%–45% (w/v) Sucrose density gradients were freshly prepared in SW41 ultracentrifuge tubes (Beckman) using a Gradient Master (BioComp Instruments). Cells were pre-treated with 100 µg ml⁻¹ cycloheximide for 3 min at 37 °C followed by washing using ice-cold PBS containing 100 µg ml⁻¹ cycloheximide. Cells were then lysed in polysome lysis buffer. Cell debris were removed by centrifugation at 14,000 r.p.m. for 10 min at 4 °C. 500 µl of supernatant was loaded onto sucrose gradients followed by centrifugation for 2 h 28 min at 38,000 r.p.m. 4 °C in a SW41 rotor. Separated samples were fractionated at 0.75 ml min⁻¹ through an automated fractionation system (Isco) that continually monitors OD₂₅₄ values. An aliquot of ribosome fraction were used to extract total RNA using Trizol LS reagent (Invitrogen) for real-time PCR analysis.

RNA-seq and m⁶A-seq. For m⁶A immunoprecipitation, total RNA was first isolated using TRIzol reagent followed by fragmentation using freshly prepared RNA fragmentation buffer (10 mM Tris-HCl, pH 7.0, 10 mM ZnCl₂). 5 µg fragmented RNA was saved as input control for RNA-seq. 1 mg fragmented RNA was incubated with 15 µg anti-m⁶A antibody (Millipore ABE572) in 1 × IP buffer (10 mM Tris-HCl, pH 7.4, 150 mM NaCl, and 0.1% Igepal CA-630) for 2 h at 4 °C. The m⁶A-IP mixture was then incubated with Protein A beads for additional 2 h at 4 °C

on a rotating wheel. After washing three times with IP buffer, bound RNA was eluted using 100 µl elution buffer (6.7 mM N⁶-Methyladenosine 5'-monophosphate sodium salt in 1 × IP buffer), followed by ethanol precipitation. Precipitated RNA was used for cDNA library construction and high-throughput sequencing described below.

Ribo-seq. Ribosome fractions separated by sucrose gradient sedimentation were pooled and digested with *E. coli* RNase I (Ambion, 750 U per 100 A260 units) by incubation at 4 °C for 1 h. SUPERase inhibitor (50 U per 100 U RNase I) was then added into the reaction mixture to stop digestion. Total RNA was extracted using TRIzol reagent. Purified RNA was used for cDNA library construction and high-throughput sequencing described below.

cDNA library construction. Fragmented RNA input and m⁶A-IP elutes were dephosphorylated for 1 h at 37 °C in 15 µl reaction (1 × T4 polynucleotide kinase buffer, 10 U SUPERase_In and 20 U T4 polynucleotide kinase). The products were separated on a 15% polyacrylamide TBE-urea gel (Invitrogen) and visualized using SYBR Gold (Invitrogen). Selected regions of the gel corresponding to 40–60 nt (for RNA-seq and m⁶A-seq) or 25–35 nt (for Ribo-seq) were excised. The gel slices were disrupted by using centrifugation through the holes at the bottom of the tube. RNA fragments were dissolved by soaking overnight in 400 µl gel elution buffer (300 mM NaOAc, pH 5.5, 1 mM EDTA, 0.1 U µl⁻¹ SUPERase_In). The gel debris was removed using a Spin-X column (Corning), followed by ethanol precipitation. Purified RNA fragments were re-suspended in nuclease-free water. Poly(A) tailing reaction was carried out for 45 min at 37 °C (1 × poly(A) polymerase buffer, 1 mM ATP, 0.75 U µl⁻¹ SUPERase_In and 3 U *E. coli* poly(A) polymerase).

For reverse transcription, the following oligonucleotides containing barcodes were used: MCA02, 5'-pCAGATCGTCGGACTGTAGAAGCTCTCAAGCAGAGACGGCAGCAGATTTTTTTTTTTTTTTTTTTTTTTVN-3'; LGT03, 5'-pGTGATCGTCGGACTGTAGAAGCTCTCAAGCAGAGACGGCAGCAGATTTTTTTTTTTTTTTTTTTTTTTVN-3'; YAG04, 5'-pAGGATCGTCGGACTGTAGAAGCTCTCAAGCAGAGACGGCAGCAGATTTTTTTTTTTTTTTTTTTTTTTVN-3'; HTC05, 5'-pTCGATCGTCGGACTGTAGAAGCTCTCAAGCAGAGACGGCAGCAGATTTTTTTTTTTTTTTTTTTTTTTVN-3'.

In brief, the tailed-RNA sample was mixed with 0.5 mM dNTP and 2.5 mM synthesized primer and incubated at 65 °C for 5 min, followed by incubation on ice for 5 min. The following was then added to the reaction mix: 20 mM Tris (pH 8.4), 50 mM KCl, 5 mM MgCl₂, 10 mM DTT, 40 U RNaseOUT and 200 U SuperScript III. The reverse-transcription reaction was performed according to the manufacturer's instruction. Reverse-transcription products were separated on a 10% polyacrylamide TBE-urea gel as described earlier. The extended first-strand product band was expected to be approximately 100 nt, and the corresponding region was excised. The cDNA was recovered by using DNA gel elution buffer (300 mM NaCl, 1 mM EDTA). First-strand cDNA was circularized in 20 µl of reaction containing 1 × CircLigase buffer, 2.5 mM MnCl₂, 1 M Betaine, and 100 U CircLigase II (Epicentre). Circularization was performed at 60 °C for 1 h, and the reaction was heat-inactivated at 80 °C for 10 min. Circular single-strand DNA was re-linearized with 20 mM Tris-acetate, 50 mM potassium acetate, 10 mM magnesium acetate, 1 mM DTT, and 7.5 U APE I (NEB). The reaction was carried out at 37 °C for 1 h. The linearized single-strand DNA was separated on a Novex 10% polyacrylamide TBE-urea gel (Invitrogen) as described earlier. The expected 100-nt product bands were excised and recovered as described earlier.

Deep sequencing. Single-stranded template was amplified by PCR by using the Phusion High-Fidelity enzyme (NEB) according to the manufacturer's instructions. The oligonucleotide primers qNT1200 (5'-CAAGCAGAAGACGGCAGCATA-3') and qNT1201 (5'-AATGATACGGCGACCACCGACAGGTTTCAGAGTTC TACAGTCCGACG-3') were used to create DNA suitable for sequencing, that is, DNA with Illumina cluster generation sequences on each end and a sequencing primer binding site. The PCR contains 1 × HF buffer, 0.2 mM dNTP, 0.5 µM oligonucleotide primers, and 0.5 U Phusion polymerase. PCR was carried out with an initial 30 s denaturation at 98 °C, followed by 12 cycles of 10 s denaturation at 98 °C, 20 s annealing at 60 °C, and 10 s extension at 72 °C. PCR products were separated on a non-denaturing 8% polyacrylamide TBE gel as described earlier. Expected DNA at 120 bp (for Ribo-seq), or 140 bp (for RNA-seq and m⁶A-seq) was excised and recovered as described earlier. After quantification by Agilent BioAnalyzer DNA 1000 assay, equal amounts of barcoded samples were pooled into one sample. Approximately 3–5 pM mixed DNA samples were used for cluster generation followed by deep sequencing using sequencing primer 5'-CGACAGGTTTCAGAGTTCATC AGTCCGACGATC-3' (Illumina HiSeq).

Preprocessing of sequencing reads. For Ribo-seq, the sequencing reads were first trimmed by 8 nt from the 3' end and trimmed reads were further processed by removing the adenosine (A) stretch from the 3' end (one mismatch was allowed). The processed reads between 25 nt and 35 nt were first mapped by Tophat using parameters (--bowtie1 -p 10 --no-novel-juncs) to mouse transcriptome (UCSC Genes)³². The unmapped reads were then mapped to corresponding mouse

genome (mm10). Non-uniquely mapped reads were disregarded for further analysis owing to ambiguity. The same mapping procedure was applied to RNA-seq and m⁶A-seq. For Ribo-seq, the 13th position (12 nt offset from the 5' end) of the uniquely mapped read was defined as the ribosome 'P-site' position. The RPF density was computed after mapping uniquely mapped reads to each individual mRNA transcript according to the NCBI Refseq gene annotation. Uniquely mapped reads of RNA-seq and Ribo-seq in the mRNA coding region were used to calculate the RPKM values for estimating mRNA expression and translation levels respectively. For m⁶A-seq, uniquely mapped reads in the 5'UTR were used to calculate the RPKM values for estimating the m⁶A levels.

Identification of m⁶A sites. We used a similar scanning strategy reported previously to identify m⁶A peaks in the immunoprecipitation sample as compared to the input sample⁷. In brief, for NCBI RefSeq genes whose maximal read coverage was greater than 15 in the input (RNA-seq), a sliding window of 80 nucleotides with step size of 40 nucleotides was employed to scan the longest isoform (on the basis of coding sequence (CDS) length; in the case of equal CDS, the isoform with longer 5'UTR was selected). For each window, a peak-over-median score (POM) was derived by calculating the ratio of mean read coverage in the window to the median read coverage of the whole gene body. Windows scoring higher than 3 in

the IP sample were obtained and all the resultant overlapping m⁶A peak windows in the IP sample were iteratively clustered to infer the boundary of the m⁶A-enriched region, as well as peak position with maximal read coverage. Finally, a peak-over-input (POI) score was assigned to each m⁶A-enriched region by calculating the ratio of POM in the IP sample to that in the input sample. A putative m⁶A site was defined if the POI score was higher than 3. The peak position of each m⁶A site was classified into five mutually exclusive mRNA structural regions including TSS (the first 200 nucleotides of mRNA), 5'UTR, CDS, stop codon (a 400 nt window flanking the mRNA stop codon) and 3'UTR.

m⁶A motif analysis. The m⁶A peaks with POI score higher than 10 were selected for consensus motif finding. We used MEME Suite for motif analysis³³. In brief, the flanking sequences of m⁶A peaks (± 40 nt) with POI scores were retrieved from mouse transcriptome and were used as MEME input.

31. Maroney, P. A., Chamnongpol, S., Souret, F. & Nilsen, T. W. Direct detection of small RNAs using splinted ligation. *Nature Protocols* **3**, 279–287 (2008).
32. Trapnell, C., Pachter, L. & Salzberg, S. L. TopHat: discovering splice junctions with RNA-seq. *Bioinformatics* **25**, 1105–1111 (2009).
33. Bailey, T. L. *et al.* MEME SUITE: tools for motif discovery and searching. *Nucleic Acids Res.* **37**, W202–W208 (2009).